JOURNAL OF PETROLOGY | VOLUME 53 | NUMBER 8 | PAGES 1673–1708 | 2012 | doi:10.1093/petrology/egs029

The Petrology and Geochemistry of Lavas from the Western Azores Islands of Flores and Corvo

FELIX S. GENSKE[1,2]*, SIMON P. TURNER[1], CHRISTOPH BEIER[1,2] AND BRUCE F. SCHAEFER[1]

[1]GEMOC, DEPARTMENT OF EARTH AND PLANETARY SCIENCES, MACQUARIE UNIVERSITY, SYDNEY, NSW 2109, AUSTRALIA

[2]GEOZENTRUM NORDBAYERN, UNIVERSITÄT ERLANGEN–NÜRNBERG, SCHLOSSGARTEN 5, D-91054 ERLANGEN, GERMANY

RECEIVED MAY 26, 2011; ACCEPTED APRIL 4, 2012
ADVANCE ACCESS PUBLICATION JUNE 19, 2012

The islands of Flores and Corvo in the Azores archipelago are the only two of nine subaerial volcanic edifices lying west of the Mid-Atlantic Ridge (MAR). This makes them important for constraining the evolution of this young (<40 Ma) oceanic plateau. The alkalic basalt suites from Flores and Corvo lie on a single liquid line of descent. Ankaramitic cumulates, with MgO contents up to ~18 wt %, result from clinopyroxene-dominated polybaric crystallization. The parental magmas (MgO ~ 11 wt %) are inferred to be low-degree partial melts (F = 3–5%) of enriched peridotite generated at depths of ~80–90 km. These primary magmas commenced crystallizing at the lithosphere–asthenosphere boundary and this continued in conduits over a pressure range of ~0·6–1·2 GPa. Only lavas with MgO < 3 wt % fractionated at shallow crustal levels. Nd and Sr isotope data reveal variations in the source of both magmatic systems, suggesting variable contributions from both enriched (E-) and depleted (D-) mid-ocean ridge basalt (MORB)-source mantle components. This is supported by the greater variability of incompatible trace-element ratios within the Flores lavas (e.g. Ba/Nd, La/Sm, Th/Nd), whereas those from Corvo exhibit a good correlation between key trace-element ratios [e.g. $(La/Sm)_N$, Th/Nd] and Sr isotope ratios. Lavas from Flores display a greater variability in Sr and Nd isotope compositions and define a mixing array between an E-MORB source and a common Azores mantle source. The latter signature is restricted to lava suites from the north and east of Flores. We concur with the generally accepted notion that Flores and Corvo are derived from the same mantle plume as is responsible for the eastern Azores islands. However, there is evidence (different Nb/Zr, Ta/Hf and La/Sm, but homogeneous Sr and Nd isotopic composition) that these two islands are dominated by a source component that is not as evident in the eastern archipelago.

KEY WORDS: *Azores plateau; magmatic differentiation; polybaric fractionation; oceanic lithosphere; OIB*

INTRODUCTION

Volcanic systems on young intraplate ocean islands have been widely studied to gain insights into the composition of the upper, and possibly lower, mantle and therefore into the recycling of lithosphere-derived components. Some of the best-studied ocean island basalts (OIB) include those from Hawaii (e.g. Macdonald, 1968; Chen & Frey, 1983; Clague, 1987; Watson & McKenzie, 1991; Sobolev *et al.*, 2005) and Iceland (e.g. Gudmundsson, 2000; Skovgaard *et al.*, 2001; Kokfelt *et al.*, 2009), which are both inferred to represent the surface expressions of deep-rooted mantle plumes (Woodhead, 1992; Sleep, 2006; Zhao, 2007). Given its lower buoyancy flux, the Azores archipelago may not necessarily reflect the surface expression of a typical mantle plume (Sleep, 1990). However, numerous workers have emphasized the potential that lies in these nine islands and the nearby Mid-Atlantic Ridge (MAR) to study the dynamics associated with plume–ridge interaction (e.g. Bourdon *et al.*, 1996; Gente *et al.*, 2003; Madureira *et al.*, 2005; Shorttle *et al.*, 2010). Additionally, the Azores basalts may provide evidence for

*Corresponding author. E-mail: felix.genske@mq.edu.au

the recycling of ancient, perhaps even Archaean, lithosphere (Schaefer *et al.*, 2002; Turner *et al.*, 2007).

Current models for the Azores mantle plume are based mainly on interpretations arising from geochemical and geophysical studies of the islands to the east of the Mid-Atlantic Ridge (e.g. Abdel-Monem *et al.*, 1975; Flower *et al.*, 1976; White *et al.*, 1979; Dupré *et al.*, 1982; Madeira & Ribeiro, 1990; Turner *et al.*, 1997; Claude-Ivanaj *et al.*, 2001; Haase & Beier, 2003; França *et al.*, 2006*b*; Beier *et al.*, 2008; Beier *et al.*, 2010; Millet *et al.*, 2009; Prytulak & Elliott, 2009) and the nearby MAR (e.g. Kingsley & Schilling, 1995; Bourdon *et al.*, 1996; Yu *et al.*, 1997; Cannat *et al.*, 1999; Charlou *et al.*, 2000). The plume has been imaged to depths greater than ~240 km by seismic tomography (Montelli *et al.*, 2004) and is suggested to be centred either to the NE of the island of Terceira (Moreira *et al.*, 1999) or potentially in the vicinity of the island of Faial (Cannat *et al.*, 1999; Gente *et al.*, 2003; Shorttle *et al.*, 2010), but in either case on the eastern plateau, 150–200 km away from the MAR. The remote islands of Flores and Corvo to the west of the MAR have been much less well studied and afford a different perspective for models for the interaction of the Azores mantle plume with the MAR. Here, we present the first detailed geochemical and petrological study of Flores and Corvo to facilitate a better overall understanding of the Azores plume. A continuous polybaric fractional crystallization model appears to best describe the petrological and geochemical evolution of the volcanic suites and a unique source is identified on the basis of the trace-element and Nd–Sr isotope data.

BACKGROUND

Geological setting

The Azores islands are situated on a submarine plateau that is subdivided by the MAR into eastern and western parts. Seven of the nine islands are located to the east of the MAR on the Eurasian and African plates and only the islands of Flores and Corvo (Fig. 1) emerge from the American plate. In contrast to the eastern islands, which are dominated by NW–SE-striking structures parallel to the ultraslow Terceira Rift axis (Searle, 1980; Vogt & Jung, 2004), the two western islands lie on a NNE–SSW-trending ridge that is subparallel to the MAR (Fig. 1). The Azores archipelago is located in the vicinity of a triple junction (Krause & Watkins, 1970; Searle, 1980; Madeira & Ribeiro, 1990; Fernandes *et al.*, 2006), and there are no obvious extensional structures on the western plateau similar to those found on the eastern plateau (e.g. the Terceira Rift Axis; Vogt & Jung, 2004; Georgen, 2008; Georgen & Sankar, 2010). The geometric shape of the western plateau is clearly influenced by the MAR, resulting in predominantly north–south-striking tectonic structures. The structural influence of MAR transform faults is reflected by the linear, east–west-striking northern and southern coastal areas of Flores and Corvo (Fig. 2) together with a relative sinistral displacement of Corvo at ~1 cm a^{-1} (Baptista *et al.*, 1999). The motion of the North American plate relative to a fixed triple junction point is in a SW direction with a velocity equivalent to a 1·2 cm a^{-1} half spreading rate (Georgen & Sankar, 2010).

To date, only one submarine volcanic edifice has been identified on the western plateau and this has basalts dated at around 4·8 Ma (Ryall *et al.*, 1983). However, Gente *et al.* (2003) identified several ridges parallel to the MAR. The subsidence-corrected topography (Gente *et al.*, 2003) suggests at least one set of two seamounts roughly 50 km west of Flores and Corvo. The spatial dimensions of these appear very similar to those of the emergent islands and may be observed again on the magnetic Chron 6 ridge (~20 Ma). Gente *et al.* (2003) also showed that the Chron 6 ridge defines the westernmost boundary of the Azores plateau as suggested by east–west-directed seismic profiles and the bathymetry, both of which define a sharp drop off towards older oceanic crust (Fig. 1a, −32° to −33°W). The overall dimensions of the western Azores plateau are ~300 km from east to west and ~400 km from north to south. The thickened oceanic crust on each flank of the MAR has a similar thickness (~8–10 km) across the plateau (Krause & Watkins, 1970; Searle, 1980; Gente *et al.*, 2003; Nunes *et al.*, 2006; Beier *et al.*, 2008; Georgen & Sankar, 2010). The top 2–3 km can be attributed to the plume, and the normal crustal thickness in this area is of the order of 7–8 km. Maximum thicknesses of ~12 km are found in the vicinity of the emergent volcanoes (Luis *et al.*, 1998; Gente *et al.*, 2003).

Flores, which is the larger of the two islands (Fig. 1b), is characterized by a group of connected and overlapping stratovolcanoes with small independent caldera systems. The lack of extended fissure systems (compare the Terceira axis and the Faial horst-and-graben system), combined with the absence of a large caldera, give Flores a unique geological character in the Azores archipelago. Current constraints from K/Ar dating of the subaerial base of Flores suggest a maximum age of ~2 Ma (Azevedo & Ferreira, 1999). The major volcanic and tectonic features on Flores have been described by Azevedo & Ferreira (2006). Corvo's dominant feature is one large caldera with a diameter of around 2 km and a maximum height of 300 m. Published ages for Corvo are somewhat ambiguous. The oldest lavas at the base of the island are reported to be 1–1·5 Ma whereas the youngest ages place the Vila do Corvo flank eruption at 80 ka (França *et al.*, 2006*a*); no historical record of volcanic activity exists. Both islands represent the subaerial expressions of volcanic systems with a base as deep as 3000 m below the present-day sea level (Fig. 1b). The bathymetric map and the NE–SW profile indicate a relative distance of 30 km between the volcanic centres and also show the erosion

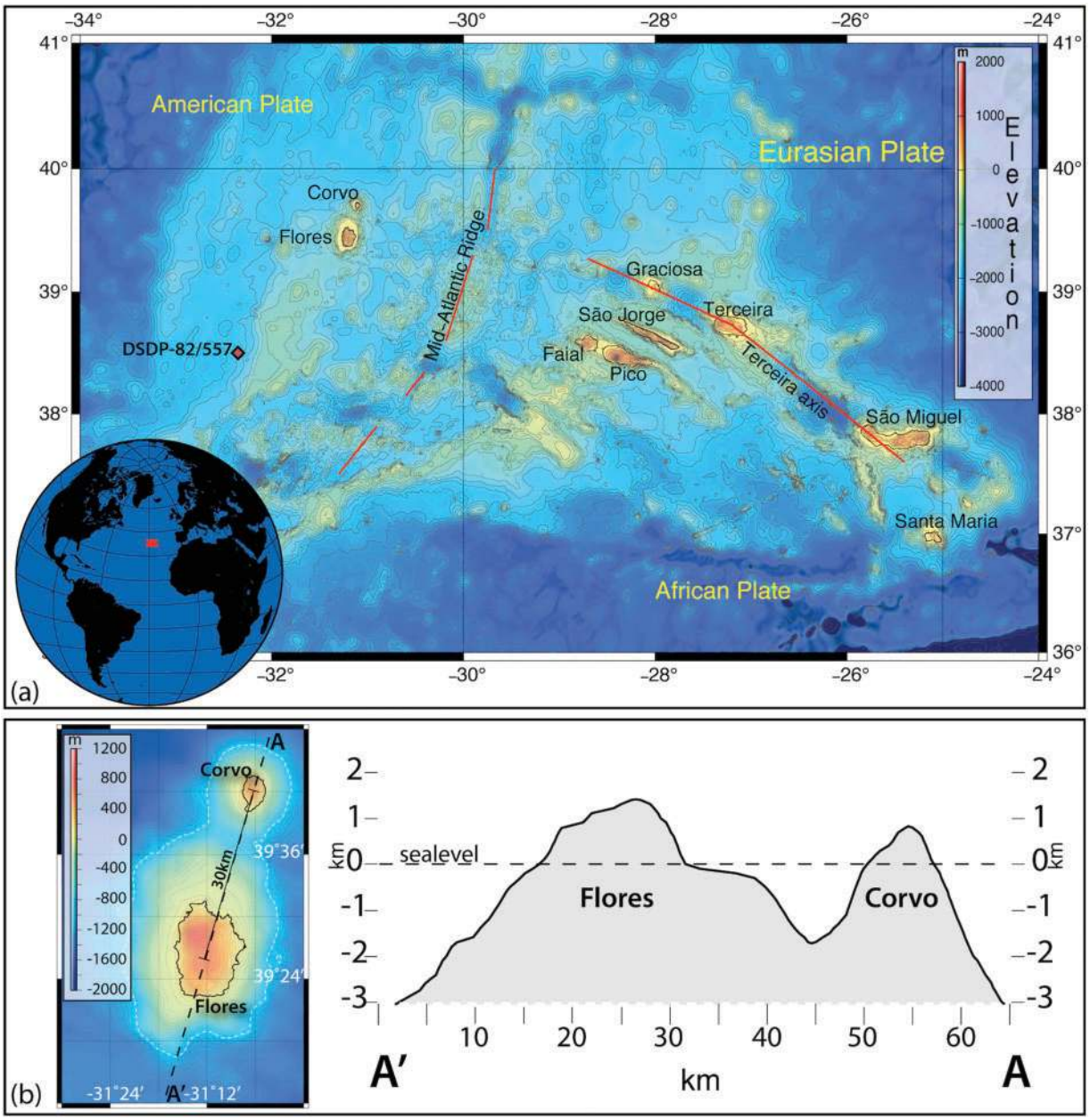

Fig. 1. (a) Bathymetric map of the Azores plateau showing the nine islands east and west of the Mid-Atlantic Ridge. (b) Bathymetric map of Flores and Corvo highlighting the emerging topography above the ocean floor. The erosion platforms on the west and NW of both volcanoes indicate the original size of both islands prior to erosion. The profile A–A′ highlights the submarine parts of the volcanic systems, which extend to depths of around 3000 m below present-day sea level. Map produced using GMT (Wessel & Smith, 1991, 1995). Vertical exaggeration is 4·75 times the horizontal.

platforms of both islands at the eastern and northern shore at ~100 m below sea level (Fig. 1).

The thick submarine volcanic packages of both islands lead to the conclusion that the age of initial volcanism must be older than 2 Ma. The magnetic stripes on the ocean floor north and south of the Azores plateau suggest that Flores and Corvo emerged from oceanic crust that is slightly younger than 10 Ma (Gente *et al.*, 2003). These age constraints, combined with plate motion of 1–1·5 cm a^{-1}, imply that the initial volcanism of the western Azores islands may have commenced when they were between 70 and 90 km from the MAR.

Stratigraphy of Flores and Corvo

The stratigraphy of Flores has previously been described by Azevedo & Ferreira (2006), and we use their

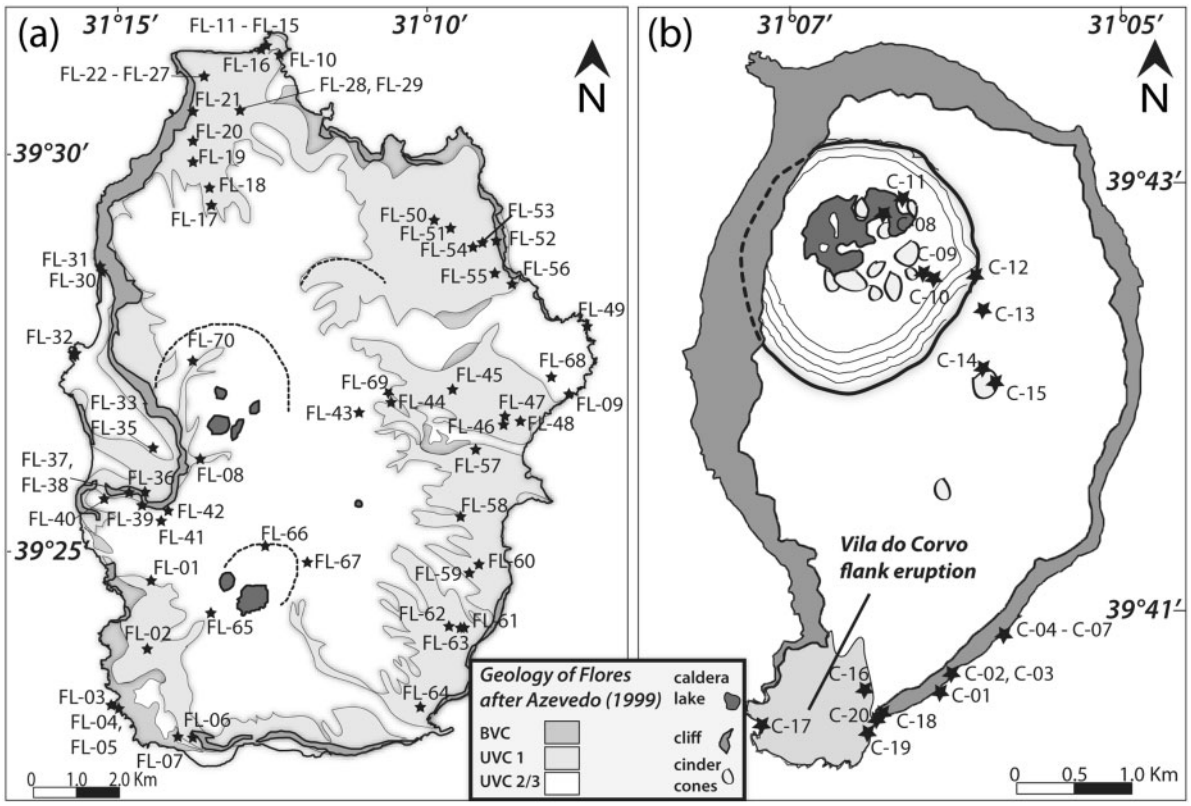

Fig. 2. Geological maps of Flores (a) and Corvo (b) indicating the sample localities from this study. The stratigraphic classification for Flores (BVC, base volcanic complex; UVC 1–3, upper volcanic complex) is taken from Azevedo & Ferreira (1999). (See text for a full description of these units.) The difference in scale between the two maps should be noted.

stratigraphic characterization herein. Because of the complexity of the volcanic system and the different styles of eruption that characterize the island, the finer stratigraphic units cannot always be ascertained, but the division into Base Volcanic Complex (BVC) and Upper Volcanic Complex (UVC1–3) is readily identifiable in the field and is illustrated in Fig. 2a. The upper complex comprises all units resulting from subaerial volcanism, whereas the BVC includes units from both submarine and emergent stages, which are largely observed in outcrops at sea level along the north and south coast. Owing to the possible interaction with seawater, the BVC rocks are mostly altered, making them mostly unsuitable for petrological and geochemical analysis. The only location where the BVC was sampled during this study was the SW coast of the island, where samples appear to be relatively unweathered and unaltered. The rocks belonging to the UVC are generally better preserved, as they form the upper section of the volcanic pile. The stratovolcanic cycles resulted in extrusive flow and fall deposits that range from basaltic lavas to trachytic scoria cones and ash layers. The eruptive styles on Flores became more explosive towards the later stages (Azevedo & Ferreira, 2006).

França *et al.* (2006*a*) have established a stratigraphic record for Corvo. Similar to Flores, it can be subdivided into a Basal (proto-island) Complex and an Upper Complex. The latter includes pre-, syn- and postcaldera deposits. The syncaldera episode is characterized by more explosive, pyroclastic flow deposits. The youngest rocks on Corvo may be associated with the Vila Nova do Corvo flank eruption. However, there are no age constraints.

ANALYTICAL METHODS

Sampling and sample treatment

The islands of Flores and Corvo were sampled in May 2009 (Fig. 2). The sampling campaign was based on observations in the field and previous stratigraphic work on Flores (Azevedo & Ferreira, 1999, 2006; França *et al.*, 2008) and Corvo (França *et al.*, 2006*a*). The aim was to sample stratigraphic profiles, two for Flores and one for Corvo, to encompass as much of the magmatic evolution of both islands as possible. Whenever possible, visibly fresh material was recovered; however, some samples collected near the shoreline show evidence of surfacial

seawater alteration. These latter samples were only investigated microscopically. For analytical work, fresh cores were cut from the unaltered samples and these were then washed and ultrasonicated in deionized water.

Electron microprobe analysis (EMPA)

Representative samples were selected for macro- and microscopical studies before electron microprobe analyses were conducted. Major-element compositions of silicate minerals were obtained using a CAMECA SX100 electron microprobe (EMP) with five fixed wavelength-dispersive spectrometers and one energy-dispersive X-ray detector at the Geochemical Analysis Unit (GAU), Macquarie University, Sydney. Cr_2O_3 and NiO concentrations were also determined for opaque phases and iron–magnesium silicates. Analyses were obtained using a focused beam, with an accelerating voltage of 15 kV and a beam current of 20 nA. Calibration standards used were albite (Na), Fe_2O_3 (Fe), kyanite (Al), olivine (Mg), chromite (Cr), spessartine (Mn), orthoclase (K), wollastonite (Ca, Si), and rutile (Ti).

Major- and trace-element analysis

Sample cores were crushed using a hydraulic press and then powdered using an agate mill to obtain a fine powder ($\ll$50 μm grain size). Thorough care was taken when cleaning the mill with Milli-Q® water and ethanol between samples to avoid cross-contamination.

Standard techniques (e.g. Potts *et al.*, 1984) were used for the major-element analysis. Glass discs for X-ray fluorescence (XRF) analysis were prepared by homogeneously fusing 0·4 g of sample with 2·5 g lithium tetraborate–metaborate flux (12:22 mixture) and ammonium iodide in a Pt crucible at 1050°C. The discs were analysed using a Spectro XEPOS energy-dispersive XRF spectrometer at the School of Earth and Environmental Sciences, University of Wollongong. Loss on ignition was determined for each sample at 1050°C for 1·5 h. Analyses of international rock standards and the samples are listed in Table 1. Accuracy of the measured values was generally better than 0·9%.

For the trace-element analyses standard methods (e.g. Eggins *et al.*, 1997) were employed. Approximately 100 mg of sample ($n = 37$) was weighed into clean 15 ml Savillex® Teflon beakers. Samples were digested using a 1:1 mixture of HF (Merck, suprapur grade) and HNO_3 (Ajax) at 160°C for 24 h, then dried down and repeated. To fully dissolve any spinel in the samples, a HF–HCl–$HClO_4$ mix was added to the digestion procedure for 2 days at 160°C. This step was repeated when necessary. After drying down at 200°C the samples were then further digested in 6N HNO_3 for 24 h, dried down again, and diluted to 10 ml in 2% HNO_3 with trace HF. Then 1:1000 dilutions of each sample were individually spiked with a 15 μl aliquot of a solution of Li, As, Rh, In, Tm and Bi in 2% HNO_3. Samples and standards were analysed by quadrupole inductively coupled plasma mass spectrometry (ICP-MS) on an Agilent 7500c/s system at the GAU, Macquarie University, Sydney. BCR-2 was used as a calibration standard to correct for instrument sensitivity and run drift. The background was measured on a 2% HNO_3 rinse solution. Measured values and the deviation from reference values from GeoReM (Jochum & Nohl, 2008) for standards BIR-1 and BHVO-2 are given in Table 1. The full dataset for the analysed samples (including Sr and Nd isotopes) is given in Electronic Appendix 1, which is available for downloading at: http://www.petrology.oxfordjournals.org).

Sr and Nd isotopes

Purification of Sr and Nd was carried out for whole-rock samples ($n = 17$) and international rock standards (~140 mg) using powders digested in Teflon beakers with concentrated HF and HNO_3. Samples were then dried down and ~1 ml of concentrated $HClO_4$ was added, followed by 4 ml 6N HCl and H_2O_2. These were dried down once again, dissolved in 6N HCl, dried, dissolved in HCl and HF, and centrifuged to remove any undissolved residue. The samples were then loaded onto Teflon columns using Biorad® AG50W-X8 (200–400 mesh) cation exchange resin and eluted using a 2·5N HCl–0·1N HF solution. Sr was collected from the column followed by Nd. Neodymium was further purified from Sm, Ba, La and Ce using a second column [Eichrom® Ln spec resin (50–100 μm)] following the methods described by Pin & Zalduegui (1997).

Isotopic analyses of Sr and Nd were obtained by thermal ionization mass spectrometry (TIMS) using a Thermo Finnigan Triton system at the GAU, Macquarie University, Sydney. Sr was loaded onto single rhenium filaments with a Ta activator and analysed between 1380 and 1430°C in a static measurement mode with rotating amplifiers. Measured $^{87}Sr/^{86}Sr$ ratios for BHVO-2 are listed in Table 1. NIST SRM 987 was analysed for instrument sensitivity during times of the analyses ($n = 17$) and gave a long-term reproducibility of $^{87}Sr/^{86}Sr = 0{\cdot}710250$ (2SD = 0·000034). Ratios were normalized to $^{86}Sr/^{88}Sr = 0{\cdot}1194$ to correct for mass fractionation.

Nd was loaded as a nitrate onto double rhenium filaments and analysed with an evaporation filament current of 1200–1600 mA and a signal of 0·5–10 V. Reference materials BHVO-2 and JMC 321 ($n = 15$) were also analysed, yielding $^{143}Nd/^{144}Nd$ ratios close to published values (Table 1). External precision was determined using JMC 321, which gave $^{143}Nd/^{144}Nd = 0{\cdot}511115$ (2SD = 0·000047) during the time of the analyses. Ratios were normalized to $^{146}Nd/^{144}Nd = 0{\cdot}7219$ to correct for mass fractionation.

Table 1: Major-element, trace-element and Nd–Sr isotope date for selected lavas from Flores and Corvo and international rock standards

Sample no.:	C-09-01	C-09-02	C-09-06	C-09-07	C-09-08	C-09-10	C-09-13	C-09-17.1	C-09-17.2	C-09-18	C-09-19	C-09-20
Island:	Corvo	Corvo	Corvo	Corvo	Corvo	Corvo	Corvo	Corvo	Corvo	Corvo	Corvo	Corvo
Lat. (°N):	39·6752	39·6766	39·6802	39·6802	39·7128	39·7081	39·7051	39·6727	39·6727	39·6736	39·6718	39·6718
Long. (°W):	31·1036	31·1025	31·0963	31·0963	31·1079	31·1029	31·0982	31·1215	31·1215	31·1089	31·1108	31·1108
Elevation (m):	2	2	2	5	412	460	546	5	5	5	5	5
Volcano-stratigraphy:	pre-caldera	caldera	pre-caldera	pre-caldera	caldera	caldera	caldera	VDC	VDC	pre-caldera	VDC	pre-caldera
TAS classification:	Alkali basalt	Tephrite	Alkali basalt	Tephrite	trachy-andesite	Tholeiite basalt	Tholeiite basalt	Trachy-andesite	Picro-basalt	Tephrite	Tephrite	Tephrite
wt %												
SiO_2	45·54	47·06	45·15	45·18	48·50	46·55	46·07	56·08	41·05	44·56	46·82	45·52
TiO_2	2·43	3·10	2·66	1·98	2·97	1·33	1·50	1·03	2·99	2·58	3·13	2·30
Al_2O_3	13·99	16·33	13·79	12·48	16·34	7·60	10·12	18·85	11·76	14·90	16·46	12·74
Fe_2O_3	11·33	12·02	12·12	10·71	11·33	9·10	9·31	7·99	14·13	12·05	11·77	11·32
MnO	0·18	0·22	0·18	0·16	0·19	0·15	0·14	0·24	0·17	0·19	0·22	0·17
MgO	9·27	4·23	8·76	11·49	3·27	18·18	15·52	1·23	10·67	8·08	4·29	10·74
CaO	12·06	8·61	11·94	13·90	6·34	14·92	14·61	4·16	15·29	12·04	8·35	13·21
Na_2O	3·12	5·10	3·28	2·89	4·16	1·08	1·51	6·48	1·67	3·55	5·59	2·32
K_2O	1·17	1·97	1·12	0·45	2·67	0·37	0·48	2·99	0·13	1·18	1·86	0·88
P_2O_5	0·49	0·84	0·49	0·30	0·94	0·20	0·25	0·50	0·17	0·45	1·11	0·39
LOI	0·41	0·77	0·35	0·80	2·98	0·70	0·75	0·43	2·01	0·75	0·05	0·40
Total	99·99	100·25	99·82	100·34	99·69	100·18	100·26	99·98	100·04	100·33	99·65	99·99
ppm												
Sc	32·2	12·8	30·3	42·7	14·3	66·5	55·9	2·71	58·9	28·8	12·6	41·7
V	268	213	327	297	172	282	264	11·7	625	338	184	321
Cr	456	21·9	418	697	24·0	2530	1414	2·04	716	226	3·71	625
Co	49·1	28·8	51·0	55·0	25·3	77·0	59·4	7·45	72·5	52·5	26·8	57·9
Ni	182	11·3	186	190	17·1	595	356	0·89	95·9	151	3·44	235
Cu	161	35·1	127	95·9	42·0	172	114	7·73	53·8	121	19·3	91·9
Zn	81·0	105	82·5	67·6	121	64·3	53·6	131	115	83·0	111	78·8
Mo	1·54	2·61	1·76	0·97	2·20	0·51	0·70	3·31	4·67	1·93	3·07	1·41
Rb	26·5	48·0	28·9	10·9	61·5	7·10	9·66	54·1	2·59	28·7	56·2	23·9
Sr	541	738	560	426	694	272	293	770	573	593	949	499
Y	24·9	38·9	26·0	20·0	38·6	17·0	16·4	41·7	20·2	24·9	42·9	24·8
Zr	185	306	181	126	347	94·6	98·4	591	84·8	177	325	166
Nb	64·8	109	60·2	35·9	124	31·2	30·2	200	11·6	61·8	131	56·4
Cs	0·28	0·40	0·26	0·37	0·40	0·14	0·09	0·13	0·03	0·29	0·69	0·23
Ba	380	629	384	245	573	182	191	1158	110	381	613	349
La	38·0	63·6	36·2	23·5	63·4	17·6	19·3	106	18·4	36·2	74·3	37·0
Ce	73·0	122	69·1	46·4	119	36·6	37·1	191	29·4	69·7	144	67·3
Pr	8·62	15·3	8·38	5·82	14·2	4·50	4·65	20·6	4·45	8·27	17·6	8·42
Nd	32·8	54·7	32·3	23·3	52·1	18·3	18·5	65·5	19·4	31·4	62·4	32·0
Sm	6·36	10·2	6·38	4·90	9·78	3·95	3·89	10·6	4·67	6·09	11·8	6·28
Eu	2·02	3·14	2·03	1·53	2·88	1·22	1·21	3·34	1·51	1·95	3·49	2·00
Gd	5·71	8·89	5·73	4·62	8·52	3·66	3·65	8·30	4·53	5·45	10·38	5·71
Tb	0·80	1·26	0·81	0·68	1·20	0·47	0·50	1·28	0·62	0·76	1·51	0·82
Dy	4·36	6·67	4·42	3·60	6·31	2·85	2·87	6·64	3·60	4·17	7·75	4·37
Ho	0·79	1·25	0·82	0·69	1·19	0·47	0·50	1·34	0·59	0·76	1·49	0·81
Er	2·14	3·35	2·17	1·78	3·14	1·31	1·36	3·73	1·59	2·04	3·84	2·12
Yb	1·71	2·68	1·72	1·40	2·54	0·98	1·06	3·58	1·14	1·61	3·15	1·67
Lu	0·19	0·34	0·20	0·19	0·33	0·12	0·09	0·57	0·14	0·18	0·45	0·19
Hf	3·81	5·81	3·66	2·97	6·52	2·31	2·30	10·6	2·92	3·52	7·03	3·62
Ta	3·95	6·69	3·64	1·93	7·42	2·20	1·69	18·7	0·62	3·58	11·24	4·08
Pb	2·36	3·30	1·62	1·35	5·10	0·83	0·85	7·38	0·47	1·68	3·89	1·58
Th	4·67	7·71	4·22	2·62	8·59	1·90	2·05	16·7	0·65	4·05	10·54	4·01
U	1·25	1·94	1·02	0·65	2·13	0·52	0·55	4·21	0·44	1·10	2·63	1·01
$^{87}Sr/^{86}Sr$	0·70335	0·70339	0·70343		0·70334		0·70350			0·70337	0·70330	0·70341
$^{143}Nd/^{144}Nd$	0·51292	0·51293	0·51292		0·51293		0·51294			0·51292	0·51292	0·51292

(continued)

Table 1: Continued

Sample no.:	FL-09-01	FL-09-07	FL-09-09	FL-09-19	FL-09-20	FL-09-23	FL-09-26	FL-09-32	FL-09-38	FL-09-41	FL-09-42	FL-09-58	FL-09-59
Island:	Flores	Flores	Flores	Flores	Flores	Flores	Flores	Flores	Flores	Flores	Flores	Flores	Flores
Lat. (°N):	39·4100	39·3769	39·4480	39·4985	39·5023	39·5149	39·5149	39·4581	39·4285	39·4226	39·4244	39·4224	39·4094
Long. (°W):	31·2451	31·2373	31·1308	31·2317	31·2316	31·2281	31·2281	31·2645	31·2512	31·2417	31·2399	31·1634	31·1602
Elevation (m):	356	151	59	359	303	100	95	6	284	460	472	350	278
Volcano-stratigraphy:*	UVC1	BVC	UVC2/3	UVC1	UVC1	UVC1	UVC1	UVC2/3	UVC1	UVC2/3	UVC2/3	UVC1	UVC1
TAS classification:	Trachy-basalt	Trachyte	(altered basalt)	Tephrite	Alkali basalt	Alkali basalt	Alkali basalt	Trachy-basalt	Trachy-basalt	Alkali basalt	Alkali basalt	Alkali basalt	Tephrite
wt %													
SiO_2	47·64	62·11	41·74	46·90	44·03	46·71	47·42	44·89	46·70	46·35	44·80	45·13	44·53
TiO_2	2·21	0·62	3·12	3·11	3·61	1·76	1·82	2·79	2·50	1·82	2·24	2·97	3·47
Al_2O_3	16·31	17·95	17·83	16·61	16·19	15·74	16·00	15·30	16·30	13·59	14·63	15·49	15·80
Fe_2O_3	10·46	3·97	13·84	11·24	13·18	11·11	11·14	12·09	11·55	10·74	11·42	11·85	12·68
MnO	0·19	0·19	0·27	0·20	0·19	0·17	0·17	0·18	0·20	0·17	0·18	0·19	0·19
MgO	6·67	0·50	3·36	4·22	5·52	8·79	7·57	7·91	5·76	10·50	9·30	6·42	6·45
CaO	9·81	1·35	5·57	7·88	10·27	11·15	11·80	10·02	10·36	11·61	10·77	10·38	10·75
Na_2O	3·74	6·14	4·32	4·51	2·58	2·61	2·77	4·36	4·08	3·16	2·78	2·78	3·34
K_2O	1·45	5·35	1·63	2·06	1·27	0·61	0·62	1·30	1·45	1·14	1·09	0·78	1·37
P_2O_5	0·61	0·14	1·67	1·33	0·86	0·43	0·43	0·70	0·76	0·46	0·64	0·65	1·01
LOI	1·15	1·69	6·36	1·79	2·00	1·09	0·38	0·31	0·38	0·01	1·92	3·11	0·67
Total	100·24	100·01	99·71	99·85	99·70	100·17	100·12	99·85	100·04	99·55	99·77	99·75	100·26
ppm													
Sc	25·4	1·56	12·9	16·7	23·3	30·8	33·0	22·9	23·0	35·5	33·0	29·2	27·0
V	216	8·56	100	211	336	207	219	249	253	252	253	327	310
Cr	255	1·86	3·03	13·0	42·1	367	232	419	141	671	572	197	116
Co	39·0	1·92	22·6	22·7	40·6	46·2	43·8	45·6	35·4	51·7	48·6	43·5	42·0
Ni	106	0·56	2·57	7·18	30·6	175	113	147	66·5	246	209	82·4	56·9
Cu	64·3	5·67	18·7	27·5	46·7	63·9	80·5	54·3	56·3	96·1	93·5	95·4	56·6
Zn	94·2	84·9	103	100	104	74·3	77·6	90·5	93·2	68·0	76·4	89·8	103
Mo	2·12	0·50	1·09	2·23	1·87	0·82	0·97	2·35	2·43	1·89	1·35	1·98	0·41
Rb	36·4	50·2	28·1	46·9	27·4	10·1	11·0	29·0	34·4	32·6	27·7	5·40	32·3
Sr	666	99·7	654	956	866	446	484	768	698	556	627	726	915
Y	49·8	14·7	41·6	42·5	33·6	21·8	25·1	26·8	30·1	24·0	25·5	30·6	34·4
Zr	246	521	304	322	225	118	120	221	200	158	160	249	228
Nb	81·2	151	104	97·0	66·4	33·4	34·7	72·4	77·4	57·9	61·2	85·2	72·7
Cs	0·39	0·36	0·22	0·20	0·19	0·04	0·10	0·30	0·47	0·43	0·20	0·17	0·16
Ba	615	1061	1079	755	464	310	307	495	585	467	528	490	540
La	72·9	24·5	53·3	68·4	44·7	22·3	24·5	42·1	42·8	33·2	36·9	50·6	46·9
Ce	95·5	46·9	111	139	87·1	45·6	47·9	80·5	84·0	64·3	70·7	98·4	95·1
Pr	14·3	5·39	15·5	18·0	11·2	5·93	6·22	9·71	10·3	7·75	8·67	12·3	12·5
Nd	51·9	18·6	60·8	68·3	44·8	23·9	24·9	36·8	39·6	29·4	33·1	43·9	48·5
Sm	9·26	3·31	12·4	13·0	9·05	4·95	5·15	7·09	7·55	5·65	6·33	8·10	9·64
Eu	3·08	1·19	4·63	4·43	3·16	1·82	1·87	2·40	2·63	1·90	2·17	2·55	3·39
Gd	9·10	2·84	11·05	11·05	8·08	4·66	4·94	6·12	6·57	5·08	5·62	6·97	8·26
Tb	1·30	0·44	1·59	1·57	1·15	0·67	0·72	0·85	0·93	0·74	0·81	1·01	1·16
Dy	6·74	2·75	7·91	7·75	5·75	3·74	4·03	4·54	4·93	3·95	4·20	5·12	5·67
Ho	1·37	0·55	1·48	1·43	1·06	0·69	0·76	0·81	0·90	0·75	0·79	0·97	1·00
Er	3·51	1·66	3·66	3·47	2·63	1·84	2·03	2·16	2·43	1·99	2·07	2·46	2·49
Yb	2·66	1·62	2·80	2·57	1·90	1·46	1·61	1·68	1·91	1·64	1·67	1·97	1·71
Lu	0·39	0·21	0·39	0·35	0·25	0·16	0·18	0·22	0·26	0·21	0·21	0·26	0·22
Hf	5·12	9·78	5·96	6·19	4·59	2·43	2·48	4·26	3·73	3·08	3·10	4·85	4·20
Ta	6·59	11·97	7·72	7·47	5·76	2·30	2·28	5·97	6·18	4·06	4·30	6·26	5·64
Pb	2·17	5·19	3·21	2·91	1·99	0·94	0·92	2·15	1·88	1·51	1·60	2·09	1·84
Th	5·44	6·67	7·39	6·49	4·04	1·89	1·92	4·59	4·16	3·58	3·55	5·24	3·52
U	1·62	1·03	1·90	1·73	0·91	0·55	0·54	1·24	1·16	0·97	0·94	1·12	0·78
$^{87}Sr/^{86}Sr$	0·70339		0·70351	0·70350	0·70355	0·70326	0·70331	0·70343	0·70337	0·70333	0·70337	0·70353	0·70350
$^{143}Nd/^{144}Nd$	0·51294		0·51291	0·51290	0·51290	0·51295	0·51294	0·51292	0·51292	0·51292	0·51293	0·51291	0·51290

(continued)

Table 1: Continued

Sample no.:	BHVO-1	Deviation	BIR-1	Deviation	BHVO-2	Deviation
wt %						
SiO_2	50·06	0·12	48·09	0·13	49·32	0·58
TiO_2	2·79	0·08	0·97	0·01	2·67	0·06
Al_2O_3	13·77	0·03	15·76	0·26	13·53	0·03
Fe_2O_3	12·34	0·11	11·51	0·21	12·03	0·27
MnO	0·17	0	0·17	0·01	0·16	0·01
MgO	7·25	0·02	9·69		7·17	
CaO	11·57	0·17	13·58	0·28	11·23	0·17
Na_2O	2·27	0·01	1·79	0·03	2·71	0·49
K_2O	0·52	0	0·02	0·01	0·51	0·01
P_2O_5	0·29	0·02	0·03	0·01	0·29	0·02
LOI						
Total	101·03		101·61		99·62	

Sample no.:	*n*	BHVO-2	2SD
$^{87}Sr/^{86}Sr$	22	0·703480	0·000034
$^{143}Nd/^{144}Nd$	19	0·512976	0·000015

Sample no.:	BHVO-1	Deviation†	BIR-1 ($n=3$)	Deviation†	BHVO-2 ($n=3$)	Deviation
ppm						
Sc			47·4	4·41	35·0	2·97
V			329	10·1	324	7·13
Cr			391	0·43	303	23·3
Co			54·5	2·49	46·3	1·34
Ni			197	31·1	137	17·6
Cu			152	33·5	168	40·8
Zn			68·2	3·77	102	0·82
Mo			0·04	0·03	4·31	0·31
Rb			0·22	0·02	9·39	0·28
Sr			109	0·38	402	5·80
Y			17·3	1·72	29·0	3·00
Zr			14·9	0·86	185	12·5
Nb			0·55	0·00	19·9	1·83
Cs			0·00	0·00	0·10	0·00
Ba			6·43	0·71	132	1·39
La			0·58	0·03	15·5	0·35
Ce			1·88	0·04	38·0	0·48
Pr			0·34	0·03	5·44	0·09
Nd			2·35	0·03	24·7	0·19
Sm			1·07	0·05	6·23	0·16
Eu			0·46	0·07	2·03	0·04
Gd			1·88	0·01	6·34	0·10
Tb			0·32	0·04	0·95	0·03
Dy			2·50	0·01	5·28	0·03
Ho			0·55	0·01	0·99	0·01
Er			1·68	0·02	2·54	0·00
Yb			1·57	0·08	1·93	0·07
Lu			0·18	0·07	0·20	0·08
Hf			0·57	0·01	4·35	0·01
Ta					1·25	0·11
Pb			2·99	0·11	1·61	0·01
Th			0·03	0·00	1·24	0·02
U			0·01	0·00	0·41	0·01

*Volcano-stratigraphy from Azevedo & Ferreira (1999).
†Deviation refers to preferred GeoRem values (Jochum & Nohl, 2008).

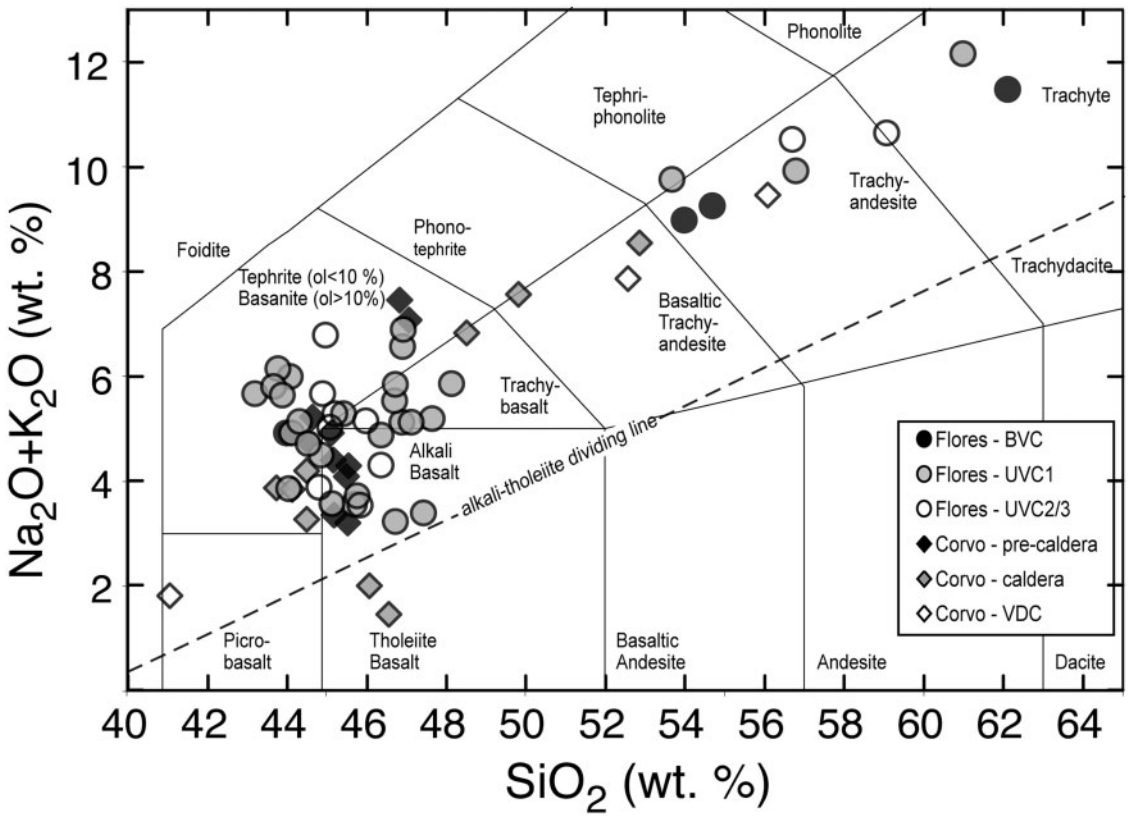

Fig. 3. Volatile-free total alkalis vs SiO_2 (TAS) diagram with the IUGS classification after Le Maitre *et al.* (1989). The stratigraphic subdivisions for Flores are adopted from Azevedo & Ferreira (2006). The dividing line between alkaline and tholeiitic compositions is from Macdonald (1968).

RESULTS

Petrography

The rocks analysed from both islands range in composition from alkali basalt to trachyte following the TAS classification of Le Maitre *et al.* (1989) (Fig. 3). However, three basalts plot in the tholeiitic basalt field and were identified in the field as clinopyroxene-dominated cumulate rocks. The broad trend that characterizes the more primitive rocks narrows in TAS compositional space towards the more evolved trachyte compositions (Fig. 3). No compositional gap is observed on either island. A summary of the petrography of representative samples is given in Table 2.

Primitive lavas and ankaramitic cumulates

The primitive rocks from both islands are alkali-basalts, with the exception of three tholeiitic basalts (two from Corvo and one from Flores), which are characterized by megacrysts of clinopyroxene and olivine. The basalts encompass a range in MgO contents between 5 and 18 wt %, though the rocks from Corvo are generally more primitive than those from Flores. The xeno- and phenocrysts of olivine, clinopyroxene and plagioclase are notably larger (up to 2 cm) in the Corvo basalts (Table 2). The matrix of all the basalts is cryptocrystalline to finely crystalline and plagioclase-dominated. Glass is absent in the groundmass, but small melt inclusions can be found in the iron–magnesium silicate phases. However, these melt inclusions cannot be linked to any specific generation of these minerals (i.e. xeno- or phenocryst). Olivines and clinopyroxene are usually normally zoned. The Corvo samples with MgO concentrations higher than 12 wt % (e.g. samples C-09-03, –05, –10 and –13) show evidence, such as aggregation and the xenomorphic shape of the crystals (Fig. 4e), for accumulation of olivine and clinopyroxene. Xenocrystic olivines have corroded cores and are often overgrown by clinopyroxene. Large xenocrysts of olivine and clinopyroxene are also found in the lower MgO Corvo basalts, but their abundance is more restricted (Fig. 4e–g).

Intermediate rocks and trachytes

The more evolved rocks from Flores and Corvo tend to belong to the younger volcanic cycles and, compared with the basalts, show greater evidence for explosive eruption styles, such as fragmented crystals and higher vesicularity

Table 2: Summarized petrography of selected samples from Flores (FL-09-xx) and Corvo (C-09-xx)

Sample	Rock type	Description of lavas
Pre-caldera stage		
C-09-01	Alkali basalt	Fresh lava flow with ~15% cpx (pheno- and xenocrystals up to 7 mm), ~5% altered Ol (<2 mm), 15% Pl phenocrysts (<3 mm), <1% Fe–Ti oxides
C-09-02	Tephrite	Highly vesicular (20%, up to 2 cm) lava, cryptocrystalline matrix with <2% Pl (<1 mm)
C-09-18	Tephrite	Lower flow of an eruption sequence, up to 1 cm sized vesicles (15%), Cpx up to 7 mm (10%), ~15% Pl phenocrysts (<1 mm) and xenocrystals (<3 mm), ~3% altered Ol, dense matrix
C-09-20	Alkali basalt	Ankaramitic basalt, fine-grained dense matrix, large vesicles (5%, <7 mm), ~10% Cpx (xenocrystals up to 2 cm), ~2% Ol, <1% Fe–Ti oxides
Caldera related		
C-09-08	Basaltic trachyandesite	Scoriaceous vesicular trachyandesite, weathered surface, glassy pumice (<2%), ~2% Pl xenocrystals
C-09-09	Alkali basalt	Fresh dense lava flow, evenly distributed Ol and Cpx (10%) up to 7 mm in size
C-09-13	Ankaramite basalt	Fresh ankaramitic flow, ~20% large idiomorphic Cpx (<1 cm), 5% altered Ol, Fe–Ti oxides disseminated in matrix (<1%)
*BVC**		
FL-09-06	Alkali basalt	Altered medium- to coarse-grained mafic composition, ~20% Pl up to 7 mm, ~20% weathered Cpx (<5 mm), relics of altered Ol (<2%)
FL-09-07	Trachyte	Massive intermediate flow, dense, ~30% Pl pheno- and xenocrystals, ~1% Bt (<1 mm)
UVC1		
FL-09-23	Alkali basalt	Fresh, vesiculated but dense basalt flow, occasional mafic cumulates (<1%), ~3% Cpx, ~3% Pl, <1% Ol, Fe–Ti oxides disseminated (≪1 mm)
FL-09-26	Alkali basalt	Fresh basaltic flow at the base of a sequence, fine-grained, ~3% Cpx (<2 mm), ~5% Pl <2 mm), ~1% Ol (<1 mm)
FL-09-59	Tephrite basanite	Scoriaceous flow, ~20% vesicles, fine-grained dense matrix, ~3% Pl, ~2% Cpx phenocrystals
UVC2–3		
FL-09-32	Trachybasalt	Fresh mafic composition, ~4% Ol xenocrystals up to 3 mm, ~2% Cpx (<3 mm), occasional (~1%) Pl laths up to 2 mm
FL-09-41	Alkali basalt	Fresh porous basalt, cm-sized Cpx ~2%, vesicular matrix, ~1% large Pl (<8 mm) xenocrystals enclosing small Cpx, ~1% Ol phenocrystals (<1 mm)
FL-09-42	Alkali basalt	Vesicular fresh basalt, ~5% Cpx up to 5 mm, ~3% Pl crystals (<3 mm), ~1% altered Ol, occasional Fe–Ti oxides

*Stratigraphy after Azevedo & Ferreira (1999).

(up to 30 vol. %). Using the TAS classification they range from trachybasalt to trachyte in composition (Fig. 3, Table 1). These rocks typically contain olivine, clinopyroxene, magnetite and plagioclase as abundant phenocrysts. A small amount of reversely zoned clinopyroxene is present in some of the trachytic lavas, but the majority (>90%) of the crystals are normally zoned, similar to the basaltic lavas. Apatite is an accessory phase in the more evolved rocks and can be found together with plagioclase and clinopyroxene phenocrysts. Olivine crystals often have iddingsitized rims and cracks that are usually filled with iron oxides. As the rocks evolve to higher silica content, plagioclase becomes more dominant (Fig. 4). Hydrous phases are observed only as alteration products of clinopyroxene in the form of kaersutitic amphiboles (Table 3) in young scoriaceous rocks in the caldera of Corvo and as pseudomorphs in young trachytic basalts on Flores.

The Vila do Corvo flank eruption and hosted cumulates

The Vila do Corvo flank eruption is thought to represent the most recent volcanic activity on Corvo (Fig. 2). Age estimates place this eruption at <80 ka (França *et al.*, 2006*a*). Based on the TAS classification, the most primitive rock analysed here is a gabbroic enclave from this flank eruption. The host lava is altered and finely crystalline to aphyric, whereas the enclave is characterized by xenomorphic crystal shapes (Fig. 4h) and is interpreted to be a

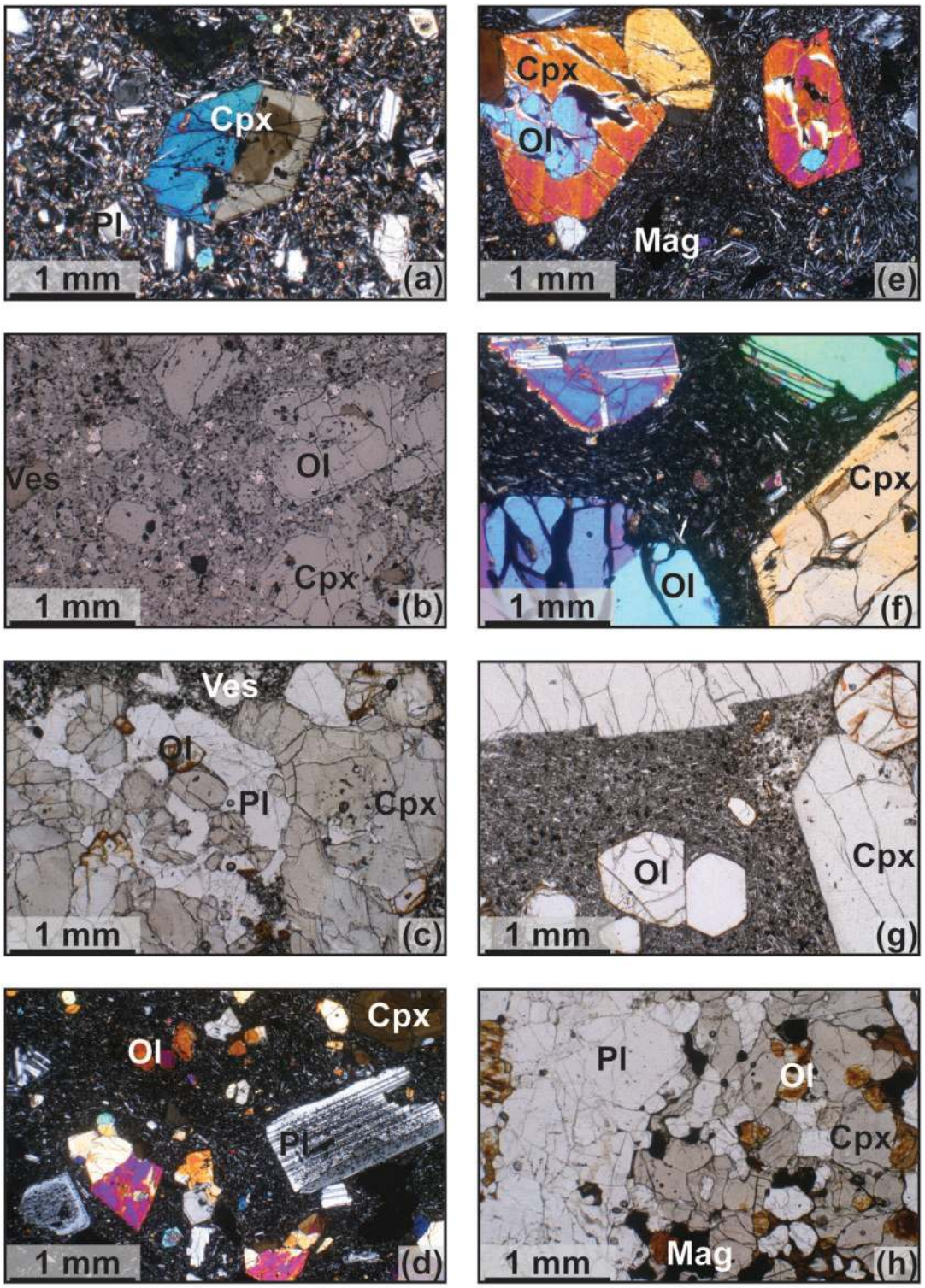

Fig. 4. Representative photomicrographs from Flores (left) and Corvo (right): (a) zoned clinopyroxene (Cpx) under crossed polars, FL-09-08; (b) opaque phases surrounding olivine (Ol) and disseminated in the matrix, reflected light, FL-09-23; (c) plagioclase (Pl), Cpx and Ol aggregate in FL-09-26; (d) inclusions in plagioclase, crossed polars, FL-09-41; (e) Ol overgrown by Cpx; magnetite (Mag) appears opaque; C-09-06; (f) Ol and hour-glass sector zoned Cpx crystals, crossed polars C-09-07; (g) ankaramitic cumulate with megacrysts of Cpx and corroded Ol C-09-13; (h) gabbroic cumulate enclave with hypidiomorphic plagioclase, olivine and clinopyroxene crystals C-09-17.2.

Table 3: Representative mineral compositions determined by EMPA

Sample no.:	LLD (wt %	C-09-01	C-09-07	C-09-10	C-09-17.2	C-09-01		C-09-07		C-09-10		C-09-17.2	C-09-08	C-09-01	C-09-07	C-09-06
Island:	oxide)	Corvo	Corvo	Corvo	Corvo	Corvo		Corvo		Corvo		Corvo	Corvo	Corvo	Corvo	Corvo
Volcano-stratigraphy:		Pre-caldera	Pre-caldera	Caldera	VDC	Pre-caldera		Pre-caldera		Caldera		VDC	Caldera	Pre-caldera	Pre-caldera	Pre-caldera
Mineral:		Ol	Ol	Ol	Ol	Cpx core	Cpx rim	Cpx core	Cpx rim	Cpx core	Cpx rim	Cpx	Kaer	Pl	Pl	Pl
SiO_2	0·08	40·01	40·81	40·21	37·52	51·92	49·63	48·88	49·29	51·73	49·47	48·32	41·25	46·95	46·67	51·74
TiO_2	0·03				0·04	0·52	1·29	1·89	1·34	0·68	1·12	2·06	5·09	0·05	0·05	
Al_2O_3	0·03		0·04	0·08	0·05	2·73	6·03	6·27	6·01	3·02	5·14	5·33	10·92	33·31	32·61	29·66
Cr_2O_3	0·06			0·08		0·98	0·39	0·10	0·70	0·40	0·62	0·06				
FeO	0·08	14·40	11·48	9·67	25·92	1·74	3·09	4·77	3·97	1·81	2·32	4·48	3·08	0·53	0·51	0·71
Fe_2O_3						2·03	1·84	1·66	1·62	2·14	2·38	2·98	14·33			
MgO	0·11	45·25	47·32	49·11	36·31	17·01	14·68	13·88	14·32	16·68	15·33	13·42	10·73			
MnO	0·06	0·23	0·21	0·17	0·50	0·07	0·09	0·12	0·12	0·11	0·07	0·21	0·43			
CaO	0·03	0·34	0·36	0·41	0·06	22·59	23·09	22·54	22·46	23·06	22·56	22·25	11·19	17·42	17·28	13·00
Na_2O	0·03				0·03	0·31	0·33	0·35	0·37	0·26	0·33	0·54	2·97	1·73	1·75	4·04
K_2O	0·03												1·21	0·08	0·08	0·25
NiO	0·09	0·09	0·21	0·30												
Total		100·38	100·47	100·06	100·43	99·94	100·51	100·47	100·24	99·93	99·37	99·65	101·20	100·08	98·98	99·46
Mg#		85	88	90	71	95	89	84	87	94	92	84				

Sample no.:	LLD (wt	C-09-08		C-09-17.2	C-09-01	C-09-05	C-09-10	C-09-08	C-09-01	C-09-05		C-09-08	
Island:	% oxide)	Corvo		Corvo	Corvo	Corvo	Corvo	Corvo	Corvo	Corvo		Corvo	
Volcano-stratigraphy:		Caldera		VDC	Pre-caldera	Pre-caldera	Caldera	Caldera	Pre-caldera	Pre-caldera		Caldera	
Mineral:		Pl	Pl	Pl	Mag-Chr	Mag-Chr	Mag	Ti-Mag	Ilm	Ilm	Ilm	Ilm	Ilm
SiO_2	0·08	61·24	54·87	47·71	0·07	0·05	0·10	0·06	0·06	0·98	0·94	0·06	0·01
TiO_2	0·03	0·04	0·09	0·04	2·16	1·30	1·92	17·19	14·00	48·41	47·82	20·65	50·38
Al_2O_3	0·03	23·61	27·98	32·24	25·58	18·65	42·05	3·50	0·94	0·50	0·32	1·82	0·06
Cr_2O_3	0·06				31·08	32·52	14·86	1·90	0·41				
FeO	0·08	0·26	0·32	0·33	19·90	22·73	13·68	41·92	8·57	36·05	35·27	11·65	32·65
Fe_2O_3					10·11	16·33	9·93	30·10	71·60	7·73	7·69	59·64	7·54
MgO	0·11				12·10	8·73	17·35	3·05	1·95	4·88	5·17	3·60	6·66
MnO	0·06							0·85	0·70	0·86	0·79	0·93	0·80
CaO	0·03	4·91	10·47	15·80	0·04			0·05	0·05	0·15	0·26	0·03	
Na_2O	0·03	8·32	5·98	2·56						0·17	0·15	0·12	
K_2O	0·03	1·46	0·35	0·10						0·10	0·10		
NiO	0·09				0·10	0·09	0·23						
Total		99·89	100·16	98·86	101·13	100·40	100·12	98·63	98·28	99·83	98·51	98·51	98·10

(continued)

Table 3: Continued

Sample:	LLD (wt	FL-09-23	FL-09-26	FL-09-41	FL-09-42	FL-09-23	FL-09-26		FL-09-41	FL-09-42	FL-09-06	FL-09-44		FL-09-23	FL-09-26
Island:	% oxide)	Flores	Flores	Flores	Flores	Flores	Flores		Flores	Flores	Flores	Flores		Flores	Flores
Stratigraphy		UVC1	UVC1	UVC2/3	UVC2/3	UVC1	UVC1		UVC2/3	UVC2/3	BVC	UVC2/3		UVC1	UVC1
Mineral:		Ol	Ol	Ol	Ol	Cpx	Cpx core	Cpx rim	Cpx	Cpx	Cpx	Kaer		Pl	Pl
SiO_2	0·08	40·74	40·33	40·25	40·60	48·70	48·11	46·82	45·30	48·89	52·26	41·30	40·48	55·39	56·79
TiO_2	0·03					1·51	2·21	2·63	2·59	1·49	0·83	5·52	5·51		
Al_2O_3	0·03	0·06	0·06	0·08	0·03	6·89	5·58	6·72	10·44	4·89	3·09	11·03	10·84	27·37	26·11
Cr_2O_3	0·06			0·06	0·09	0·36	0·09		0·10	0·18	0·23				
FeO	0·08	12·78	13·83	11·80	9·71	3·39	4·73	5·24	3·95	3·66	3·19	0·68	12·70	0·35	0·21
Fe_2O_3						2·85	2·84	3·41	3·15	3·77	0·94	13·51	0·00		
MgO	0·11	46·35	45·65	47·99	49·11	14·24	13·44	12·49	12·26	13·75	16·27	12·51	12·66		
MnO	0·06	0·16	0·18	0·14	0·14	0·15	0·19	0·19	0·17	0·16	0·08	0·47	0·45		
CaO	0·03	0·33	0·34	0·36	0·31	22·39	22·08	21·98	22·50	22·60	23·26	11·49	11·35	10·33	9·31
Na_2O	0·03					0·41	0·51	0·54	0·36	0·53	0·25	2·92	2·98	5·37	6·09
K_2O	0·03											1·03	1·02	0·32	0·42
NiO	0·09	0·20	0·22	0·19	0·19										
Total		100·69	100·71	100·89	100·19	100·93	99·78	100·02	100·84	99·94	100·41	100·48	97·98	99·14	98·93
Mg#		87	85	88	90	88	83	81	85	87	90				

Sample:	LLD (wt	FL-09-41	FL-09-42	FL-09-07		FL-09-23	FL-09-23	FL-09-26	FL-09-41	FL-09-41	FL-09-42	FL-09-42	FL09-44	FL-09-11	FL-09-69
Island:	% oxide)	Flores	Flores	Flores		Flores	Flores	Flores	Flores	Flores	Flores	Flores	Flores	Flores	Flores
Stratigraphy:		UVC2/3	UVC2/3	BVC		UVC1	UVC1	UVC1	UVC2/3	UVC2/3	UVC2/3	UVC2/3	UVC2/3	UVC1	UVC2/3
Mineral:		Pl	Pl	Kfs		Mag	Mag-Chr	Ti-Mag	Ti-Mag	Mag-Chr	Ti-Mag	Mag-Chr	Ilm	Ilm	Ilm
SiO_2	0·08	50·72	49·55	64·64	62·02	0·08	0·04	0·07	0·13	0·13	0·13	0·12	0·00	0·01	0·43
TiO_2	0·03			0·05	0·04	23·44	15·34	17·59	22·87	0·94	17·62	0·81	48·92	49·84	36·30
Al_2O_3	0·03	30·81	31·23	20·30	21·98	2·95	6·54	5·54	2·93	20·91	3·75	22·13	0·06	0·15	2·40
Cr_2O_3	0·06					4·82	17·74	0·08		41·74	0·11	41·99			
FeO	0·08	0·57	0·58	0·14	0·25	47·85	40·31	41·55	48·24	16·01	43·87	12·91	36·24	28·83	23·76
Fe_2O_3						16·98	16·04	30·27	21·80	7·20	30·11	7·10	9·33	13·21	32·38
MgO	0·11	0·14	0·12			3·40	3·94	4·18	2·58	13·04	2·47	15·17	3·56	8·49	5·33
MnO	0·06					0·73	0·66	0·49	0·94	0·44	0·70	0·38	1·60	0·81	
CaO	0·03	14·57	14·62	2·15	4·54	0·10	0·04		0·09		0·20		0·05		0·05
Na_2O	0·03	3·20	3·02	7·98	8·12				0·05				0·04		
K_2O	0·03	0·20	0·19	3·81	1·59										
NiO	0·09					0·10				0·14		0·16			
Total		100·21	99·29	99·07	98·53	100·45	100·65	99·78	99·63	100·55	98·96	100·75	99·81	101·34	100·64

Fe_2O_3 calculated assuming stoichiometry; for amphiboles after Droop (1987). LLD, lower limit of detection. VDC corresponds to Vila do Corvo flank. Stratigraphy for Flores is according to Azevedo & Ferreira (2006).

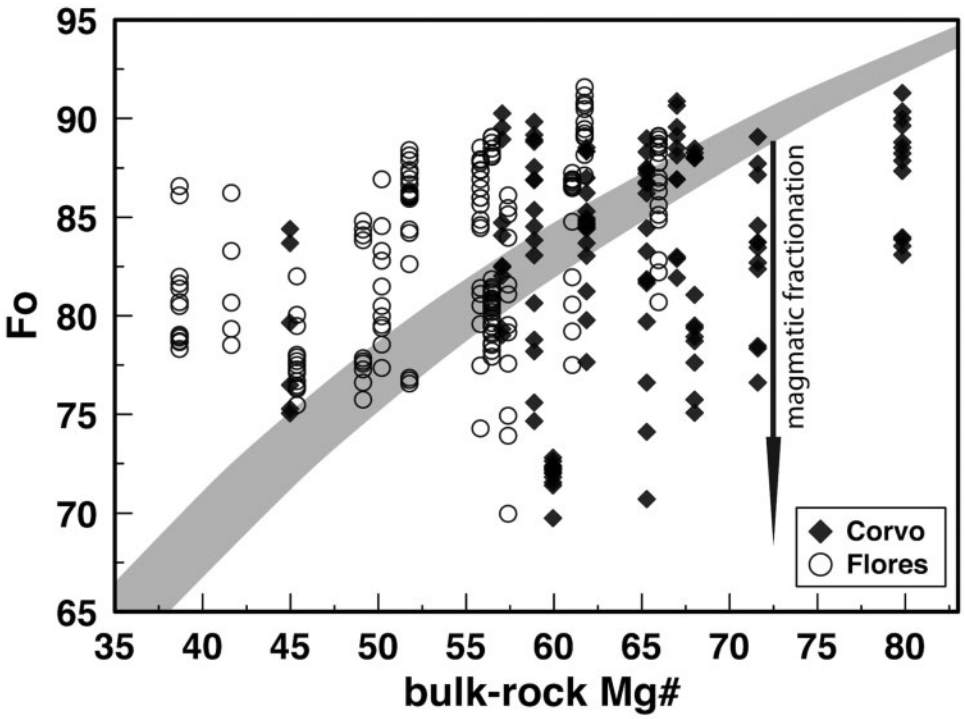

Fig. 5. Variation of the forsterite content of olivine versus bulk-rock Mg# (after Rhodes *et al.*, 1979) in single lavas from Flores and Corvo. Olivines that are in equilibrium with the host lavas plot in the grey field, where equilibrium is based on the Fe–Mg exchange coefficient between the olivine and the host lava. The K_D value used here is 0·3 (±0·03).

cumulate. Relatively unaltered samples of the host lava have evolved trachyandesite compositions, making this one of the most evolved rocks on Corvo. This flow carries abundant ovoid enclaves that vary in size from roughly fist-sized to ~30 cm. The chemical characteristics of the host lava and the enclave are summarized in Table 1.

Mineral chemistry

Olivine

A predominance of forsteritic olivines is characteristic of lavas from both islands (Table 3). The analysed olivine cores from Flores range from Fo_{69} to Fo_{91} (Fig. 5). The Corvo olivines range from Fo_{68} to Fo_{91}, whereas $Fo_{68–73}$ is typical for the olivines in the gabbroic enclave (C-09-17.2) in the Vila do Corvo flank eruption (C-09-17.1). The lavas on Corvo contain only olivines between Fo_{71} and Fo_{91}, and are characterized by normal chemical zoning. Olivine rims from both islands extend to $Fo_{\sim 64}$. In summary, the olivines from Corvo are, on average, slightly more primitive. The highest abundance of olivine crystals that are in chemical disequilibrium with the host lavas is observed for lavas with bulk-rock Mg# between 55 and 67 (Fig. 5). NiO contents increase with increasing Fo content and whole-rock Mg#. However, the NiO concentration in the most primitive olivine cores ($Fo_{89–91}$) ranges from ~1000 to 2500 ppm, which may be indicative of mixing between evolved and primitive magmas, as has also been observed in the eastern island of São Miguel (e.g. Beier *et al.*, 2006).

Clinopyroxene

The clinopyroxenes from both islands are Ti-augites (Table 3). Like the olivines, their chemical composition is very restricted and they seem to be slightly more evolved in the lavas from Flores ($Wo_{38–46}En_{41–55}Fs_{03–16}$) compared with those from Corvo ($Wo_{40–46}En_{45–55}Fs_{02–11}$). However, this compositional distinction is very subtle (Fig. 6). Most crystals are slightly zoned with decreasing MgO and increasing TiO_2 and FeO contents from core to rim, but occasionally some crystals show reverse zoning. Faint hour-glass (or sector) zoning (e.g. Vernon, 2004) is observed occasionally (Fig. 4f) but is not reflected in the composition.

Feldspar

The feldspars from both islands are predominantly plagioclase; those from Flores have a total compositional range of $Ab_{12–66}An_{41–88}Or_{0–3}$. However, the basalts with the lowest whole-rock alkali contents contain two distinct plagioclase compositions: a more primitive plagioclase generation with $An_{64–77}$ and a more evolved one with $An_{41–51}$. Only the trachytic lavas on Flores contain anorthoclase $Ab_{67–70}An_{10–13}Or_{19–23}$ (Table 3, Fig. 7). Corvo's feldspar compositional range is more restricted

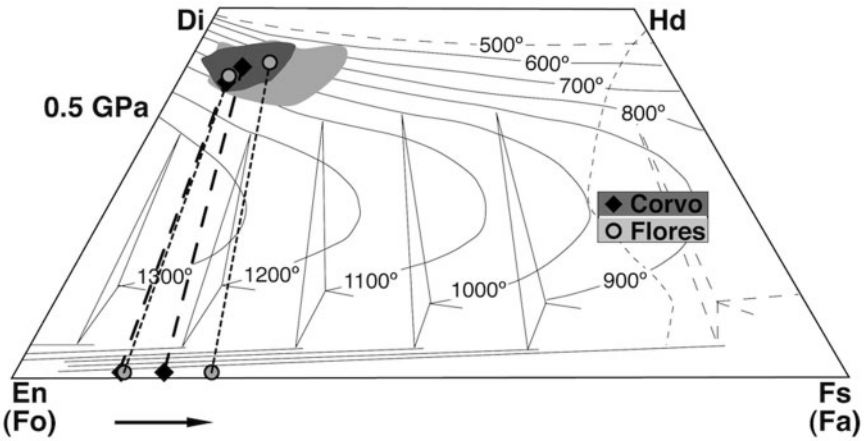

Fig. 6. Clinopyroxene compositions projected into the pyroxene quadrilateral with temperature contours after Lindsley (1983). The 0·5 GPa projection was chosen according to the pressure range obtained from samples with whole-rock MgO contents of around 5 wt %. Coexisting olivines are plotted on the En–Fs (Fo–Fa) base line for both primitive and evolved samples from both islands.

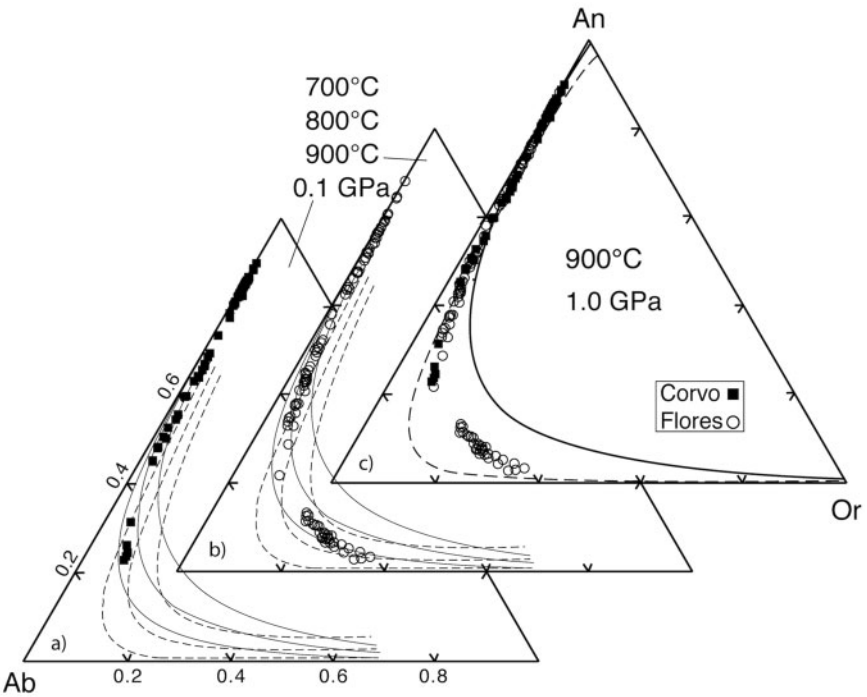

Fig. 7. Feldspar ternary diagram with temperature curves from the models of Benisek *et al.* (2010) (continuous lines) and Fuhrman & Lindsley (1988) (dashed lines). The 0·1 GPa projection reflects minimum pressure conditions, as the magmas most probably crystallize early plagioclase at greater depths and higher temperatures.

(bytownite–labradorite) and also more primitive ($Ab_{10–40}An_{60–90}Or_{0–2}$).

Fe–Ti oxides and spinels

Ilmenite, titanomagnetite and chrome-spinel are the opaque phases found in the matrix of the lavas from Flores and Corvo. They also occur around the rims of, and as inclusions in, the Fe–Mg silicates. The more mafic rocks contain proportionally more spinel (1–2%), whereas the trachytic lavas show a dominance of ilmenite (~1%) over titanomagnetite and chrome-spinel (<0·5%) (Tables 2 and 3).

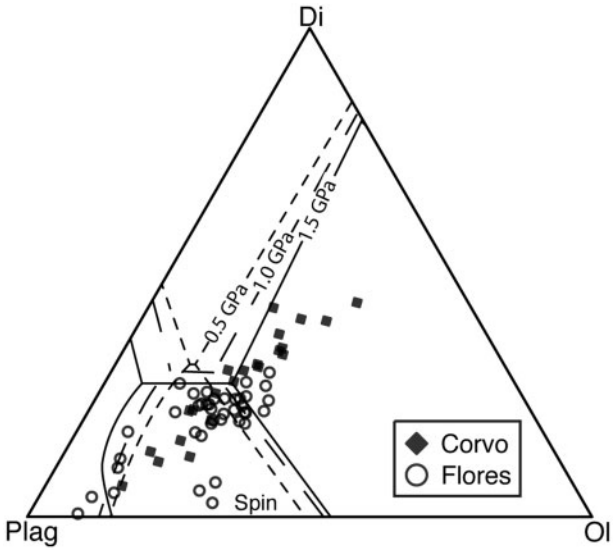

Fig. 8. Olivine–clinopyroxene–plagioclase phase diagram redrawn after Presnall *et al.* (1978), showing the calculated mineral proportions in the lavas from Flores and Corvo, determined using the method of Stolper (1980). The evolution of the lavas towards the plagioclase corner follows the change of liquidus boundaries with decreasing pressure. The three Corvo samples in the olivine field furthest away from the 1·5 GPa line represent the ankaramitic cumulates.

Amphibole

Idiomorphic to hypidiomorphic Ti-rich kaersutitic amphiboles were observed in one basaltic trachyandesite on Corvo and in one trachyte on Flores (C-09-08, FL-09-44; Table 3). These partially to completely replace original Ti-augite, which is most clearly identified by the skeletal (pseudomorphic) clinopyroxene crystal shape; however, some cores of the original augite are also occasionally preserved. The kaersutites typically exhibit opaque rims of magnetite (e.g. Deer *et al.*, 1992).

Biotite

Biotite was observed only in one mildly altered trachyte sample of the BVC unit of Flores (FL-09-07). The crystals occur in small (2–3 mm) patches around the feldspars and in the matrix. They are brown to dark brown in colour with strong pleochroism. Smaller (<1 mm) single crystals are also disseminated throughout the matrix.

Accessory phases

Apatite needles with a maximum length of 1 mm occur in the matrix and as inclusions in clinopyroxene and plagioclase, with increasing modal abundance in the intermediate to evolved rocks (1–5 wt % MgO). A few larger apatite crystals were found in the caldera scoria cones of Corvo with sizes up to 5 mm (C-09-08).

Whole-rock geochemistry

Major and trace elements

Representative whole-rock major-element data are given in Table 1. The modal olivine–clinopyroxene–plagioclase abundance in all of the lavas was calculated using the method of Stolper (1980). The results are projected onto a phase diagram (Fig. 8), after Presnall *et al.* (1978), and demonstrate a good agreement with the observed petrography. The lavas from Flores show a more variable trend when compared with those from Corvo; their average composition appears slightly more evolved.

Bivariate plots of selected major-element oxides versus MgO wt % are used to investigate the evolutionary trends for the lavas from Flores and Corvo in Fig. 9. The two islands are comparable in their overall compositional range as MgO decreases from 12 to 4 wt %. Across this range SiO_2 decreases slightly, from ~47 to 44 wt %, but then abruptly increases (up to 63 wt %) in lavas with <3 MgO (wt %) (not shown; refer to Table 1 and Fig. 3). CaO decreases over the entire MgO range with a slight positive inflection between 4 and 6 MgO wt %. P_2O_5 and TiO_2 first increase to a maximum at 4–4·5 wt % MgO, after which they decrease significantly as the compositions evolve to lower MgO (Fig. 9a and f). FeO^T ($FeO^T = 0{\cdot}8998 \times Fe_2O_3$) shows a similar trend to TiO_2; however, it does not increase as strongly between 4·5 and 12 MgO wt %. Al_2O_3 and alkali contents (Fig. 9b–d) increase towards lower MgO. A good correlation between Al_2O_3 and CaO is observed (Fig. 10a). The lavas from Flores form a dominant cluster at around 10 wt % CaO.

Both lava suites show a positive correlation between MgO and Ni and Cr concentrations at MgO higher than 4 wt % (Fig. 11a and b). Maximum Ni concentrations of 250 and 300 ppm correspond to 10·5 and 11·1 wt % MgO respectively (Table 1). Incompatible trace-element variations (La, Sr, Y, Zr) are shown in panels (c)–(e) of Fig. 11. These form negative correlations with MgO and the lowest concentrations are observed in the ankaramitic cumulate rocks from Corvo at ~15 and 18 wt % MgO. The observed trends for Corvo are better defined than the more scattered ones from the Flores suite. On Corvo, only sample C-09-17.2 deviates from the trends, and this can be explained by its gabbroic nature. The scatter in the Flores lavas cannot be attributed to relative age or location of the samples; this is discussed further below.

The same trace elements illustrated in Fig. 11 are plotted against the highly incompatible element Nb in Fig. 12. It should be noted that the *x*-axis is log-scaled to highlight the differences between the Flores and Corvo trends and to emphasize the deviation of the most primitive cumulate rocks at the lowest Nb contents. Again, relatively clean trends are observed for the Corvo suite, whereas the Flores lavas show scatter, which is greatest for Sr and Y.

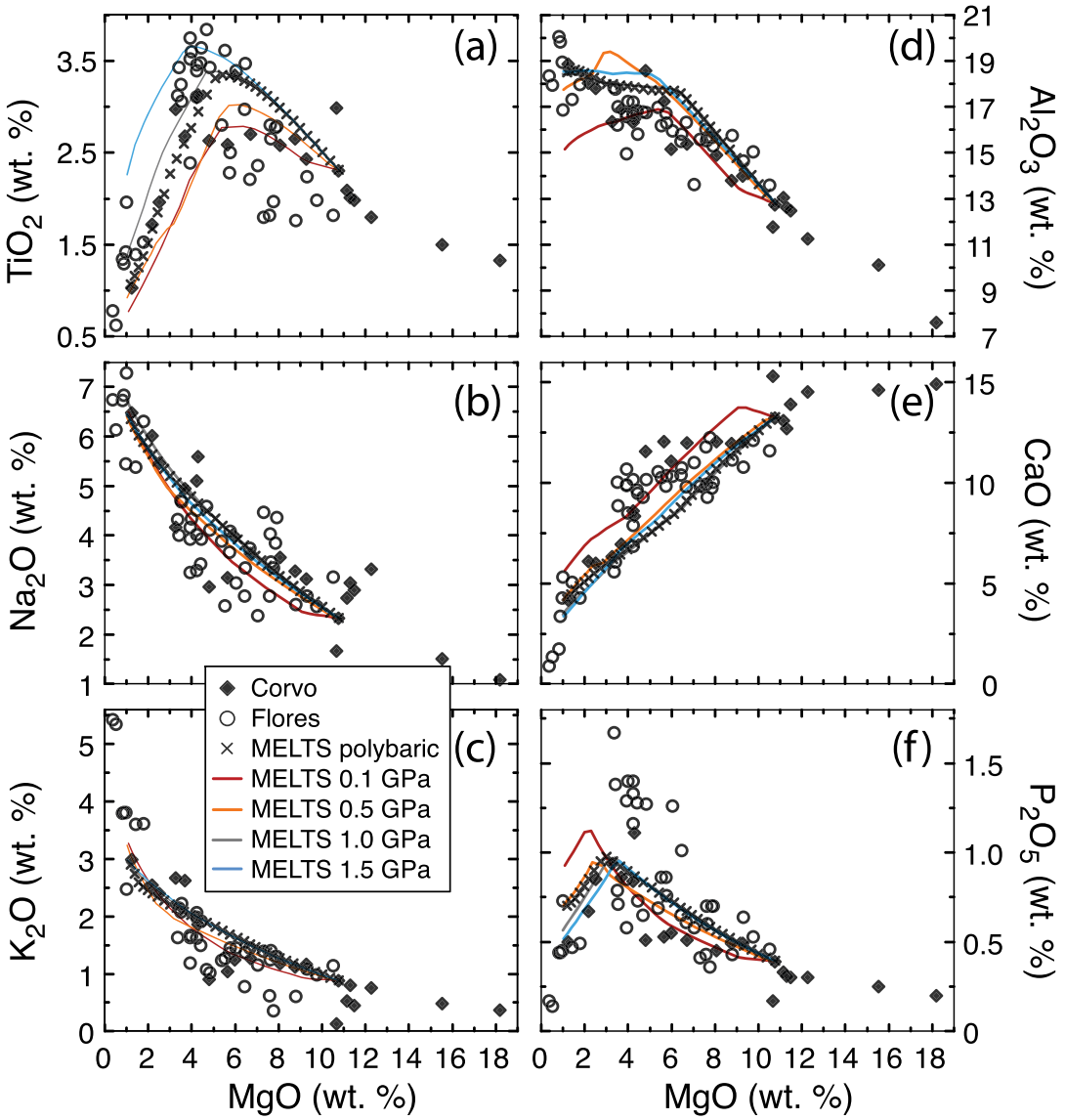

Fig. 9. Major-element contents versus MgO (wt %) for lavas from Flores and Corvo. Continuous lines represent the evolution of the liquid at different pressures modelled using the MELTS algorithm (Ghiorso & Sack, 1995; Asimow & Ghiorso, 1998), whereas the crosses represent a polybaric MELTS model. It should be noted that for all models shown, C-09-20 is the parental starting magma composition chosen for the calculations. Tick marks on the polybaric model represent 10°C intervals. (See text for full details and model parameters.)

In terms of their primitive-mantle normalized incompatible trace-element patterns (Fig. 13), the lavas from both islands are enriched in Nb–Ta and La–Ce, whereas Zr and Hf show a relative depletion. Some Flores lavas also have negative Ti anomalies. Overall, the most primitive lavas from Flores appear to be somewhat more enriched in incompatible trace elements compared with Corvo lavas with similar MgO concentrations. A slightly stronger depletion in the heavy rare earth elements (HREE) over light rare earth elements (LREE) is characteristic of Corvo.

The variation of Dy/Yb and Nd/Sr versus Dy and Nd is sensitive to the depth of partial melting and fractionation, respectively (Fig. 14). Corvo lavas have a relatively restricted range in both diagrams, whereas the data from Flores scatter significantly. However, the trends, especially for Corvo, do not back-project towards the ankaramites as clearly as in Figs 11 and 12, but still fall within the observed overall range of compositions. The Dy/Yb plot suggests that there may be two compositional groups within the Flores samples, possibly reflecting differences in the presence of residual garnet during source melting (Fig. 14a).

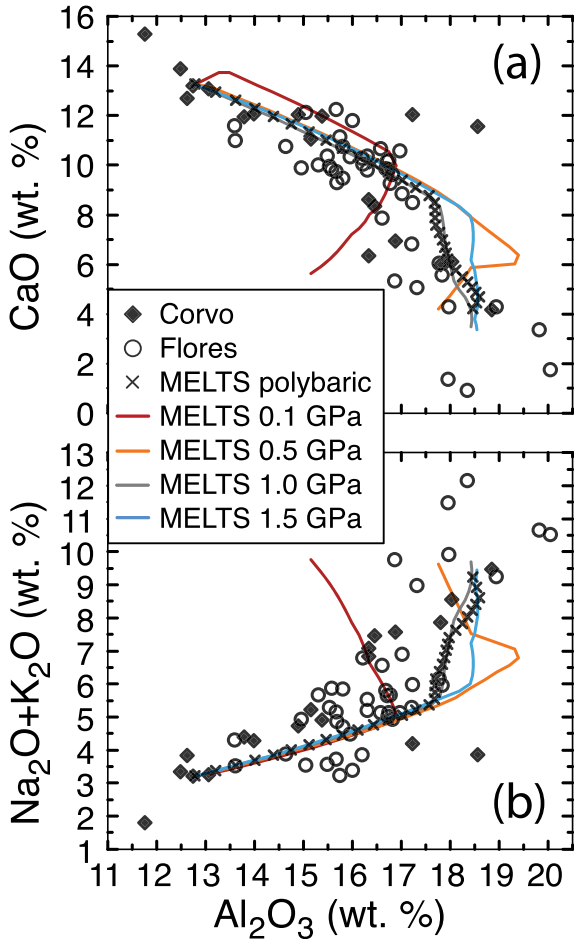

Fig. 10. Total alkalis and calcium contents versus Al_2O_3 (wt %) of Flores and Corvo lavas. Shown for comparison are model MELTS curves (see Fig. 9) at 0·1, 0·5, 1·0 and 1·5 GPa. Only samples with MgO <13 (wt %) are plotted to illustrate the models better.

Sr–Nd isotope systematics

The lavas from Corvo and Flores are very similar in their Sr and Nd isotopic compositions. Lavas from Corvo appear to be relatively invariant in their $^{143}Nd/^{144}Nd$ ratios (~0·51293), whereas the Flores lavas form a broad negative trend of $^{87}Sr/^{86}Sr$ versus $^{143}Nd/^{144}Nd$, which is comparable with data from the eastern Azores islands of Pico and São Miguel (Fig. 15). However, the Flores and Corvo data show a more restricted range in Sr and Nd isotope compositions and are more MORB-like when compared with the eastern Azores data. The most radiogenic sample in Sr from Corvo (C-09-13, $^{87}Sr/^{86}Sr \sim 0{\cdot}70350$) is interpreted to be an ankaramitic cumulate; however, seawater alteration could be the reason for this more radiogenic composition (e.g. Whipkey *et al.*, 2000). Figure 15b reveals a distinct group of lavas from Flores (red symbols) that were predominantly sampled from a section of the stratigraphic unit UVC1 around the east and north coast of the island. It should be noted that these samples are characterized by higher TiO_2 contents (refer to Table 1) and by differences in their trace-element ratios (see below). These characteristics are not restricted to samples from a discrete stratigraphic unit or location, but are found in lavas throughout the island.

QUANTIFICATION OF INTENSIVE PARAMETERS

Differentiation and crystallization of OIB is generally considered to take place near isobarically at shallow crustal depths (e.g. Widom *et al.*, 1992; Ablay *et al.*, 1998; Beier *et al.*, 2006). However, we find that there is evidence for deeper, and arguably polybaric, processes occurring beneath Corvo and Flores. We have attempted to calculate intensive parameters for this magmatic system to provide constraints for subsequent major- and trace-element models for magmatic differentiation in the western portion of the Azores archipelago.

Geothermobarometry

The iron–magnesium silicates, as well as the feldspars, from the Corvo and Flores lavas were used to estimate intensive parameters such as the pressure (P) and temperature (T) of the ascending magmas below the islands. For the calculation of these parameters only crystals in chemical equilibrium (e.g. Fig. 5) with their host-rocks were utilized. One sample from each island (C-09-08, FL-09-44) containing kaersutite phenocrysts was also used in an attempt to calculate the stability conditions of the amphibole in the shallower part of the magmatic system. A K-feldspar geothermometer was also applied to the highly evolved samples from Flores (MgO <1 wt %) to estimate the (shallowest) temperature conditions of the crystallizing magmas.

Ti-augite geothermobarometry

Geothermobarometric calculations were performed on clinopyroxene phenocryst cores using the models of Putirka (2003, 2008). Table 4 summarizes the P–T estimates from the different methods; the most consistent and statistically robust results are provided by the cpx–liquid model (Putirka, 2003). The whole-rock compositions of single lavas were used to represent the nominal liquid compositions; corresponding mineral core analyses were tested for equilibrium with that liquid before proceeding to calculate pressures and temperatures. This was achieved by comparing the stoichiometrically calculated clinopyroxene components from the lava compositions with those of the measured mineral components (Putirka, 1999). Samples whose measured and predicted components deviated strongly were not used for P–T estimates. Furthermore, mineral data that revealed Fe–Mg exchange [$K_D(Fe–Mg)^{cpx–liq}$] values outside the range of $0{\cdot}27 \pm 0{\cdot}03$ were also inferred to be out of equilibrium

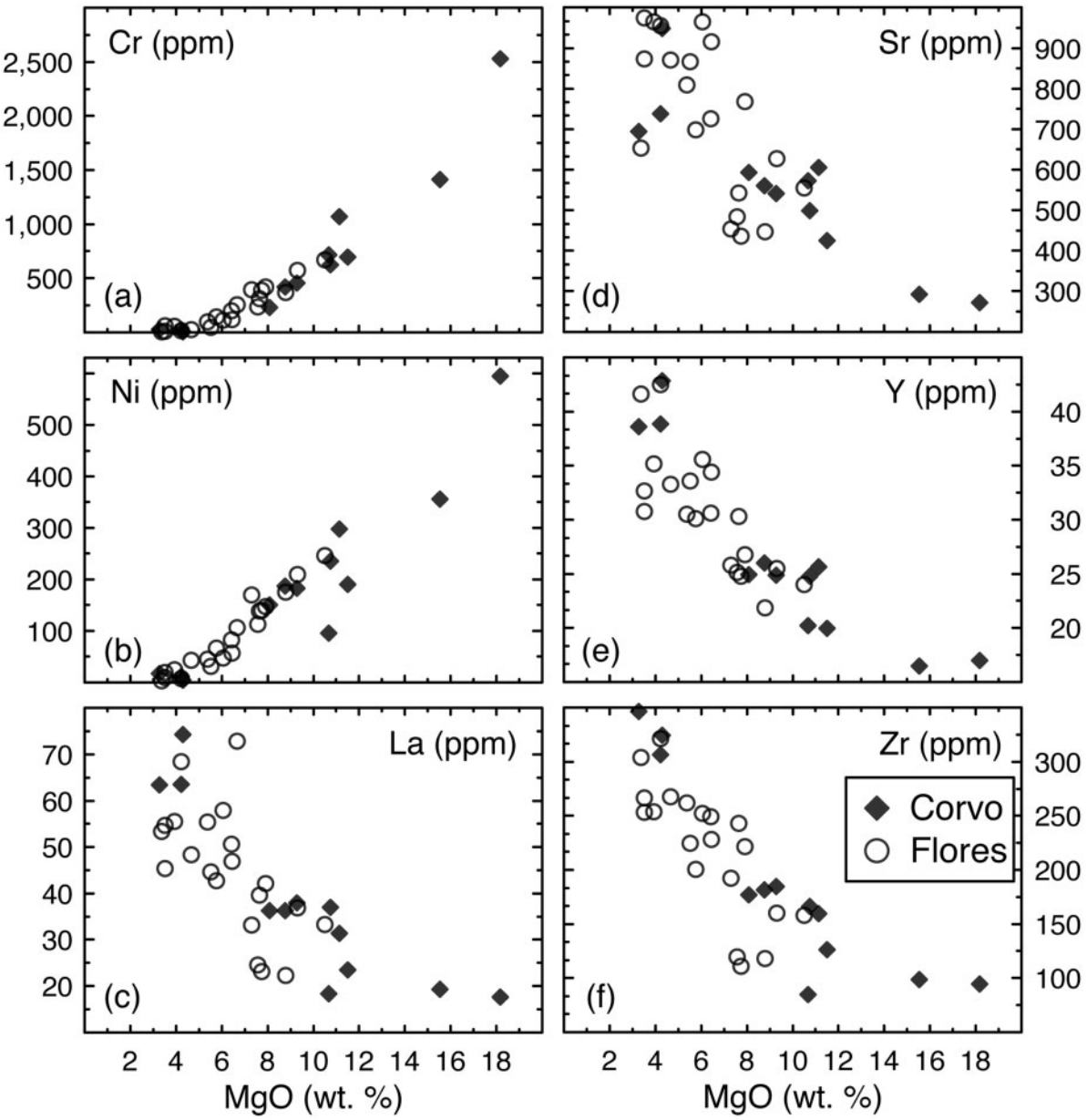

Fig. 11. Compatible (a, b) and incompatible (c–f) trace-element variations versus MgO (wt %) in the lavas from Corvo and Flores. The highest Cr and Ni contents correlate with the ankaramitic samples (C-09-10 and C-09-13). These two samples are also characterized by the lowest incompatible trace-element concentrations.

with the liquid and therefore not used for P–T estimates. Figure 16a summarizes the P–T estimates from equilibrated clinopyroxenes from Corvo and Flores. Each data point reflects a single lava, where the P–T values are based on the average compositions of corresponding equilibrated clinopyroxenes. The highest temperatures and pressures calculated for Corvo were 1302 (±6)°C and 1·19 (±0·06) GPa, respectively. Maximum values for Flores are 1256 (±9)°C and 1·05 (±0·10) GPa. Strikingly, there is a continuum towards lower P and T and thus a discrete magma chamber seems unlikely at lithospheric depths. In detail, a linear fit through the data array from each island ($R^2 > 0{\cdot}9$) suggests that the P–T gradient of the ascending magmas differs slightly between the two islands and that the magmas from Corvo appear to have a slightly deeper (*c.* +5 km) onset of crystallization than those from Flores. These observations contrast with inferences from some of the eastern islands [e.g. see Beier *et al.* (2006) for São Miguel], where two distinct and shallow magma chambers have been suggested. It should be noted that the gabbroic

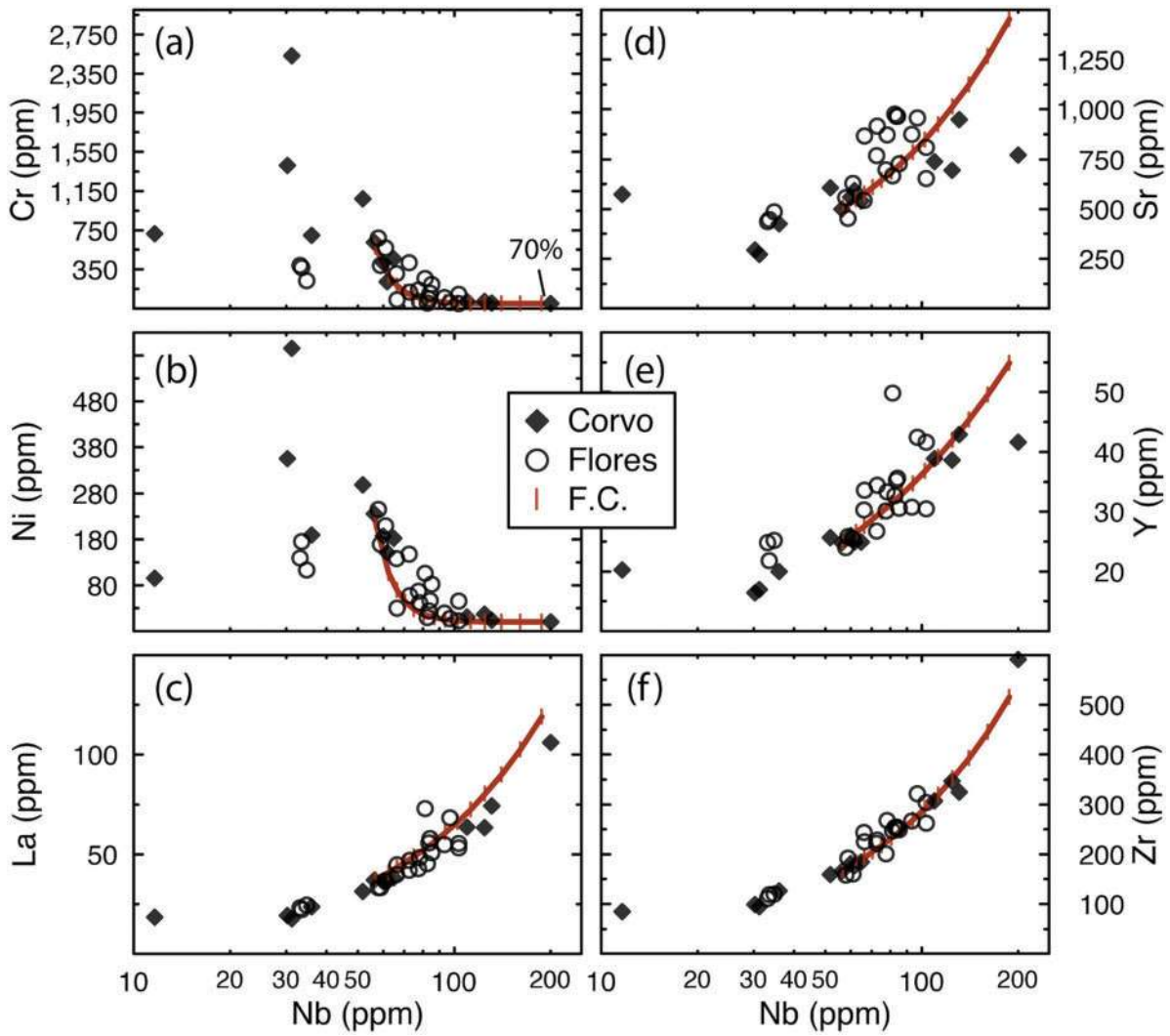

Fig. 12. Variation of Cr, Ni, La, Sr, Y and Zr versus Nb (ppm), where Nb is selected as a highly incompatible element to constrain the crystal fractionation history. A Rayleigh-fractionation model is represented by the continuous line with sample C-09-20 as the starting composition, stopping at 70% fractionation. Tick marks represent 5% increments of fractional crystallization. The fractionating assemblage used here is based on the petrographic observations and is composed of cpx–ol–plag–mag (modal %: ~30–3–5–1). Partition coefficients used to calculate the model are given in Table 7.

cumulate from the Vila do Corvo flank eruption does not allow for reliable P–T calculations owing to the heterogeneity in its mineral compositions and small size that makes it unrepresentative in terms of a whole-rock analysis.

The Ti-augites were also plotted in the pyroxene quadrilateral for a first-order approximation of the temperature conditions (Fig. 6). Because the Lindsley (1983) geothermometer is isobaric, a 1·5 GPa projection (not shown) best approximates the most primitive compositions, whereas the 0·5 GPa projection (Fig. 6) displays the best correspondence to temperatures calculated using Putirka (2008) for the more evolved (trachytic) samples. The 0·5 GPa projection is illustrated in Fig. 6, because this best reflects the crystallization depths reported for comparable ocean island settings (e.g. São Miguel, the Canary Islands, Madeira; Hansteen *et al.*, 1998; Klügel *et al.*, 2000; Schwarz *et al.*, 2004; Beier *et al.*, 2006).

Olivine thermometry

Because olivine represents one of the earliest crystallizing phases it was used to estimate the liquidus temperatures of both systems. The Putirka (2008) approach was chosen as the resulting liquidus temperatures are consistent with the observed whole-rock MgO–temperature dependence in the clinopyroxene (Fig. 16b). The Beattie (1993) model, which uses the melt composition to calculate olivine equilibrium temperatures, is consistent (±10 K) with the Putirka (2008) model. Accordingly, the liquidus

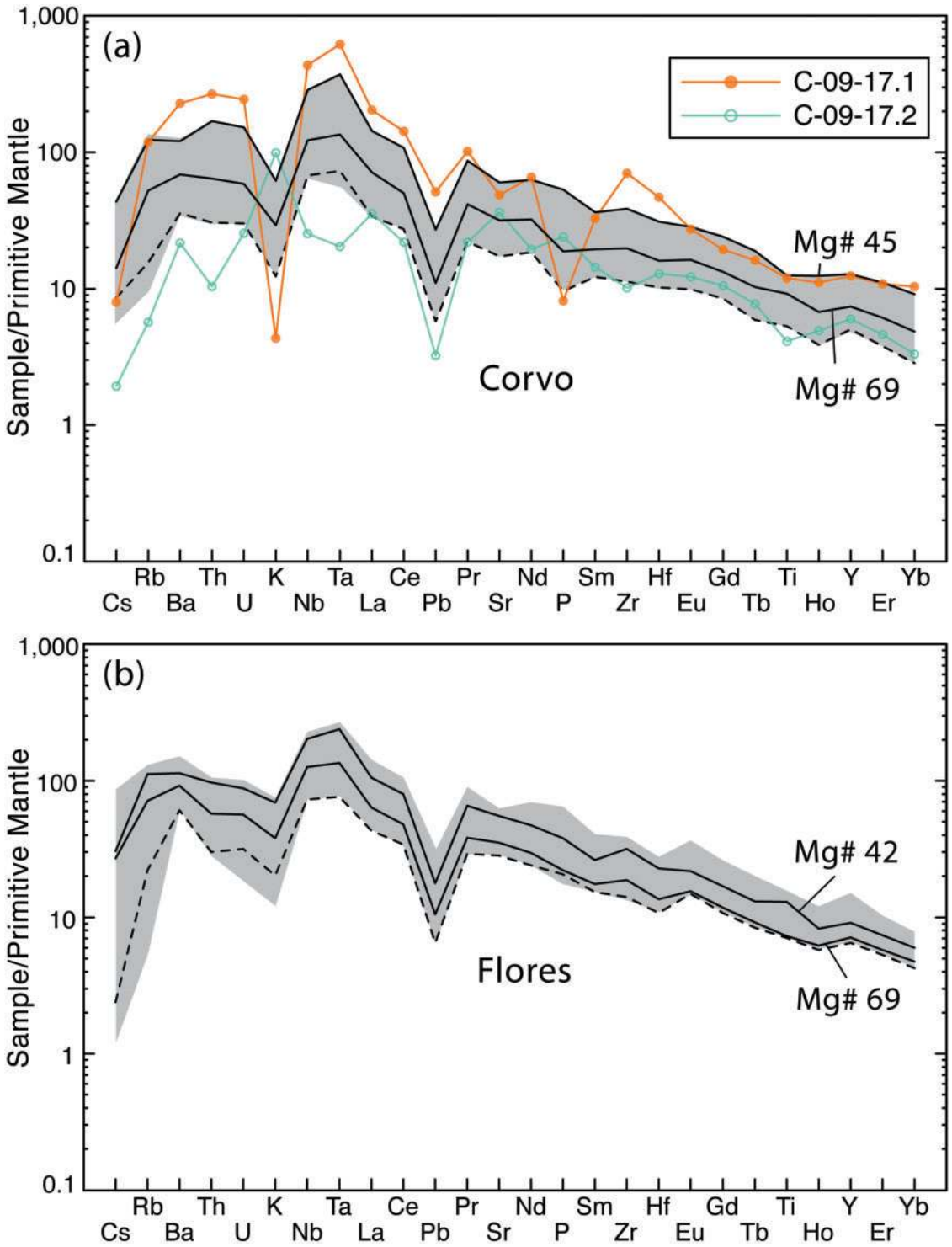

Fig. 13. Primitive mantle normalized (Sun & McDonough, 1989) multi-element plots showing (a) Corvo and (b) Flores lavas (grey fields). Each plot shows the evolution from a primitive sample (Mg# 69) towards an evolved composition (Mg# 45 and 42, respectively). Panel (a) also highlights the Vila do Corvo flank eruption showing the host lava (C-09-17.1) and the gabbroic cumulate (C-09-17.2). The dashed lines reflect accumulative rocks (ankaramites), which are more abundant in the Corvo suite. Both islands have comparable trace-element characteristics with negative K and Pb anomalies; however, slightly positive Eu and Y anomalies are more prominent in the Flores lava suite. Also, the more mobile large ion lithophile elements (Sr, Rb, Ba, K) reveal a different trace-element signature in the Flores rocks when compared with Corvo.

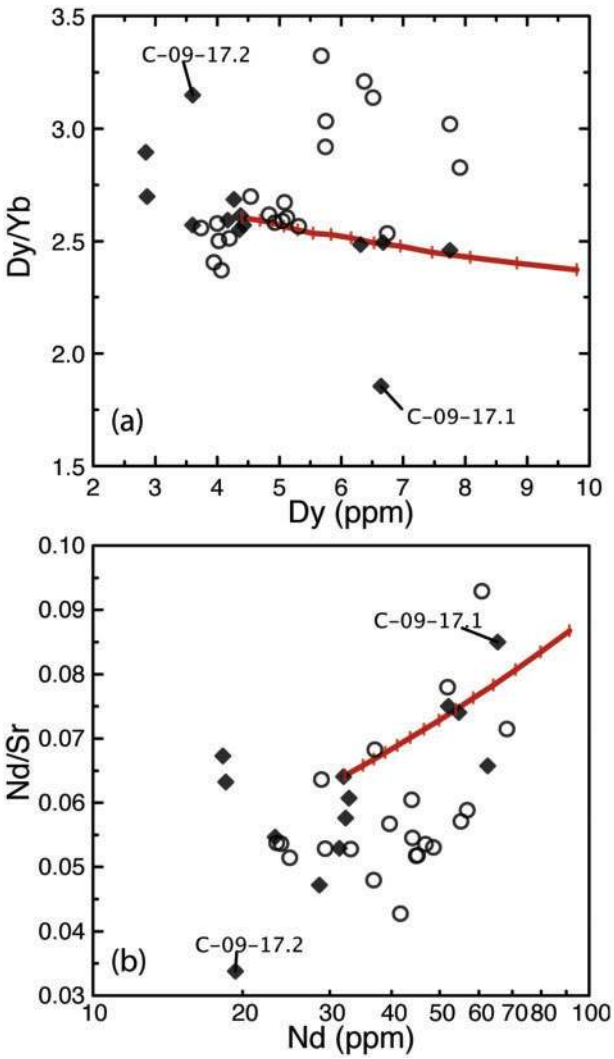

Fig. 14. Element-ratio plots for fractionation-sensitive elements in the Flores and Corvo magmatic systems. (a) Dy/Yb versus Dy indicates a similar differentiation path for both islands; however, a cluster of samples with higher Dy/Yb ratios from Flores may indicate a contribution from a different source or assimilation processes within the deep lithosphere. (b) Nd/Sr versus Nd also illustrates similar differentiation processes for both magmatic systems. The ankaramitic cumulates from Corvo have Dy < 3 ppm and Nd < 20 ppm. The Rayleigh-fractionation model shown by the continuous line uses the same parameters as that in Fig. 12. The tick marks represent 5% increments of fractional crystallization and the model trend stops at 70% total fractionation.

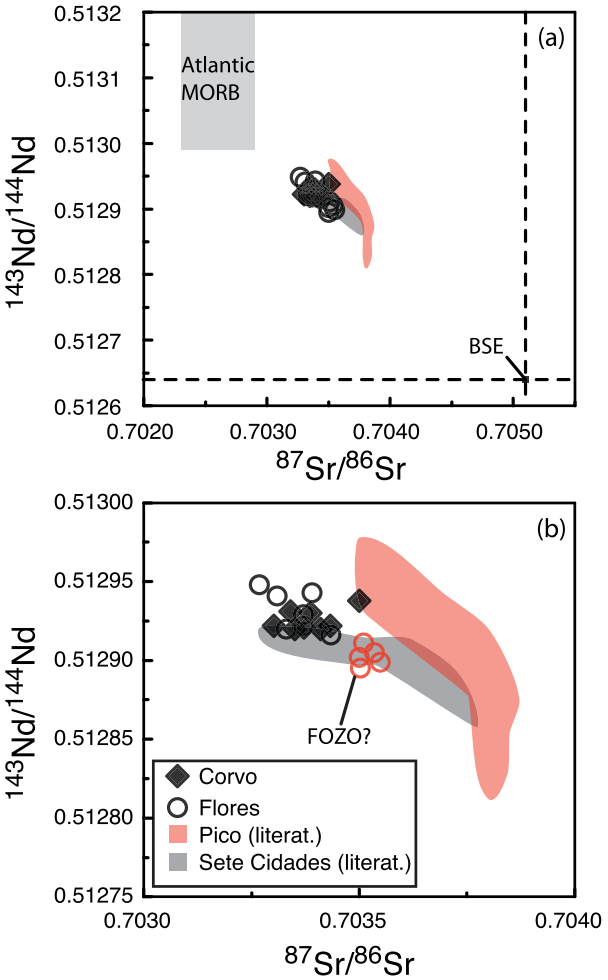

Fig. 15. Nd–Sr isotopic variations in the Flores and Corvo lavas. Literature data from Pico (red field) and Sete Cidades (São Miguel, grey field) are plotted for comparison (data from Turner *et al.*, 1997; Beier *et al.*, 2006, 2007). The samples plot within the mantle array (a) between Bulk Silicate Earth (BSE) and Atlantic MORB (data from Chauvel & Blichert-Toft, 2001). (b) Close-up of the Flores and Corvo data highlighting the differences between the two systems, with Flores trending towards more radiogenic $^{87}Sr/^{86}Sr$. A distinct group of Flores lavas is characterized as FOZO-like (red circles).

temperature of the most primitive lava from Corvo (C-09-03, 12·3 MgO wt %) is estimated to be ~1375°C (Table 4).

Amphibole and feldspar thermobarometry

To estimate the lower end of the intensive parameter range (i.e. the shallowest conditions), feldspar and amphibole thermometry was applied. Amphibole thermobarometry (Ridolfi *et al.*, 2010) provides estimates consistent with the dP/dT path determined from the ferromagnesian silicates (Table 4); the amphibole P–T parameters lie on the extrapolated path illustrated in Fig. 16a.

Feldspar thermometry was conducted using the approaches described by Fuhrman & Lindsley (1988), Benisek *et al.* (2004, 2010) and Putirka (2005). The ternary projection of the feldspar compositions onto experimentally determined temperature curves is shown in Fig. 7, where panels (a) and (b) (Corvo and Flores respectively) provide temperatures for a 0·1 GPa projection, whereas in panel (c) both islands are plotted onto a 1·0 GPa projection. Even though the 900°C isotherm does not change between the two depth projections, the process of continuous

Table 4: Geothermobarometric estimates on lavas from Flores and Corvo

Sample	MgO (wt %)	Putirka (2003) cpx–liquid				Putirka (2008) cpx (anhydr)			
		T (°C)	1SD	*P* (GPa)	1SD	*T* (°C)	1SD	*P* (GPa)	1SD
C-09-01	9·3	1238	9	0·94	0·90	1192	22	0·55	2·13
C-09-05	6·0	1166	4	0·71	0·43	1141	11	0·44	1·09
C-09-06	8·8	1222	9	0·82	0·94	1187	14	0·51	1·51
C-09-07	11·5	1302	6	1·19	0·62	1193	9	1·04	1·10
C-09-08	3·3	1074	13	0·59	1·49	1145	5	0·29	1·81
C-09-15b	11·3	1283	9	1·18	0·87	1213	23	0·89	1·84
C-09-17.2	10·7	1341	63	1·70	3·99	1205	15	1·36	9·30
C-09-18	8·1	1211	11	0·85	0·90	1159	17	0·58	1·54
FL-09-01	6·7	1186	8	0·79	0·76	1171	19	0·61	1·44
FL-09-11	4·4	1122	8	0·56	0·95	1121	23	0·35	1·42
FL-09-23	8·8	1239	10	1·04	1·02	1183	20	0·72	1·90
FL-09-41	10·5	1256	9	1·05	0·99	1211	17	0·68	1·59
FL-09-59	6·5	1179	11	0·85	1·30	1147	6	0·49	1·56
FL-09-69	5·7	1153	9	0·66	0·98	1157	18	0·49	1·25

Sample	MgO (wt %)	Fo content	Putirka (2008) ol–liquid			Beattie (1993) melt (ol)		
			1SD	*T* (°C)	1SD	*n* =	*T* (°C)	Diff. from Putirka
C-09-01	9·3	84·6	0·7	1308	3	14	1311	3
C-09-03	12·3	89·7	0·9	1375	8	2	1374	−2
C-09-05	6·0	75·2	0·1	1230	1	2	1235	5
C-09-06	8·8	83·0	1·7	1299	5	4	1302	3
C-09-07	11·5	88·2	0·2	1349	1	5	1353	3
C-09-15b	11·3	87·6	0·8	1356	5	4	1362	6
C-09-18	8·1	81·8	1·0	1284	3	4	1286	2
C-09-20	10·7	87·0	0·5	1332	2	6	1334	3
FL-09-01	6·7	80·7	0·8	1253	7	4	1257	5
FL-09-20	5·5	76·1	0·5	1208	2	4	1210	2
FL-09-23	8·8	85·2	0·6	1287	0	2	1293	5
FL-09-26	7·8	82·2	1·5	1257	4	3	1256	−1
FL-09-32	7·9	80·5	0·8	1292	3	19	1299	7
FL-09-41	10·5	86·6	1·0	1336	3	7	1344	8
FL-09-58	6·4	76·7	0·2	1244	1	3	1236	−8
FL-09-59	6·5	78·7	1·0	1238	3	4	1242	4
FL-09-69	5·7	77·4	1·0	1228	3	7	1230	2

Sample	MgO (wt %)	Putirka (2008) K-fsp–liquid			Ridolfi *et al.* (2010) amph				
		T (°C)	1SD	*n* =	*T* (°C)	1SD	*P* (GPa)	1SD	*n* =
C-09-08	3·3				960	22	0·30	0·33	1
FL-09-07	0·5	920	1	8					
FL-09-44	0·9				1003	14	0·31	0·21	25
FL-09-60	0·4	926	3	17					

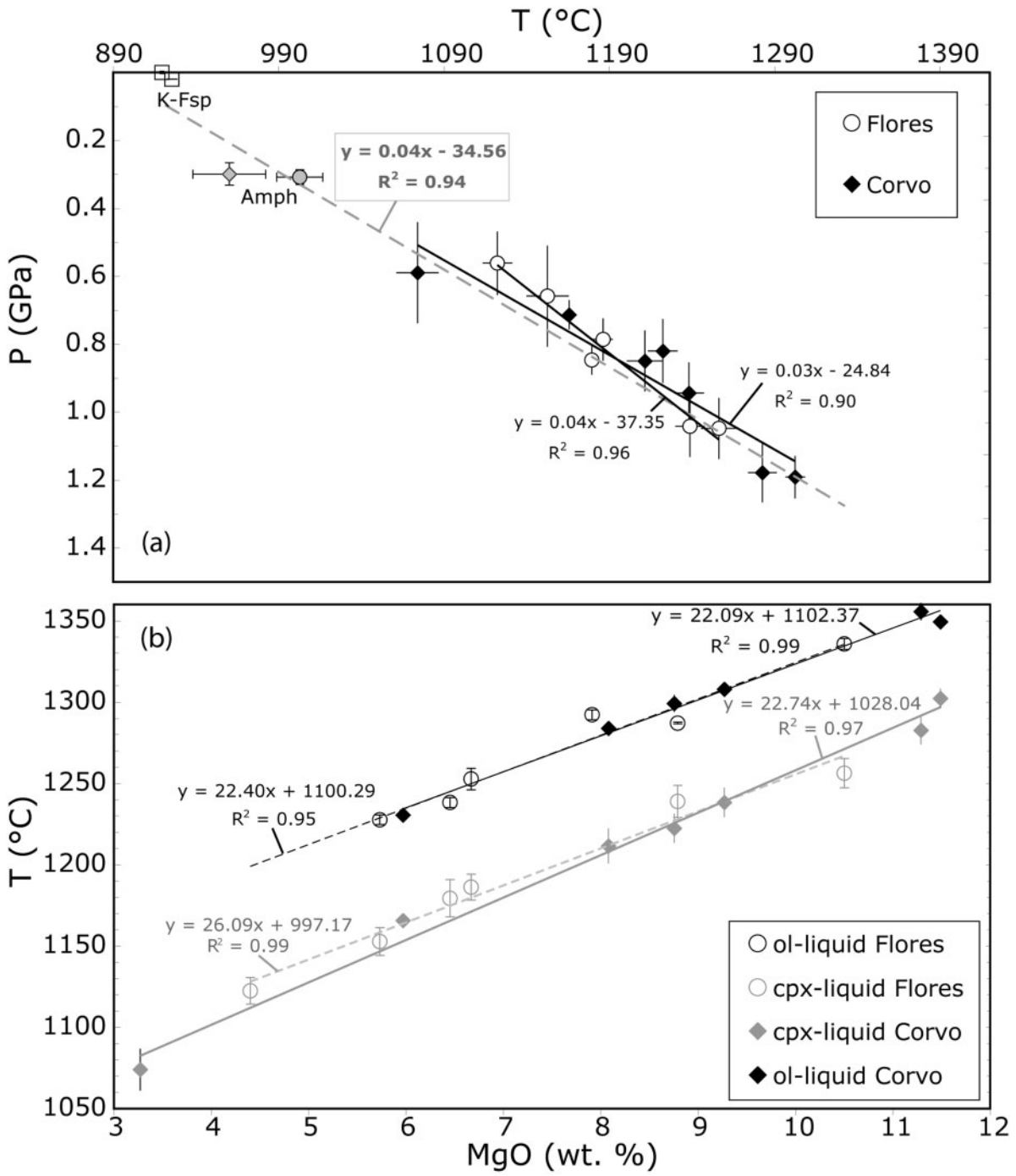

Fig. 16. Temperature and pressure estimates from equilibrium minerals (summarized in Table 4). (a) Approximate P–T path for the lavas from Corvo and Flores during clinopyroxene-dominated differentiation. Clinopyroxene, amphibole and K-feldspar were used for these calculations. The grey dashed P–T path is a summary of Flores and Corvo clinopyroxenes (linear regression, $R^2 \sim 0{\cdot}9$), as they are the most abundant phase and therefore the calculated values are statistically more robust. Amphibole and K-feldspar intensive parameters are plotted for information only, but appear to confirm the trend (linear regression through all clinopyroxene P–T estimates). (b) Temperature vs MgO content (wt %) of the lavas highlighting the consistency between olivine- and clinopyroxene-derived temperature paths. Regression lines here correspond to Flores (dashed lines) and Corvo (continuous lines), each with R^2 values >0·9, which may imply continuous P–T evolution of the magmas.

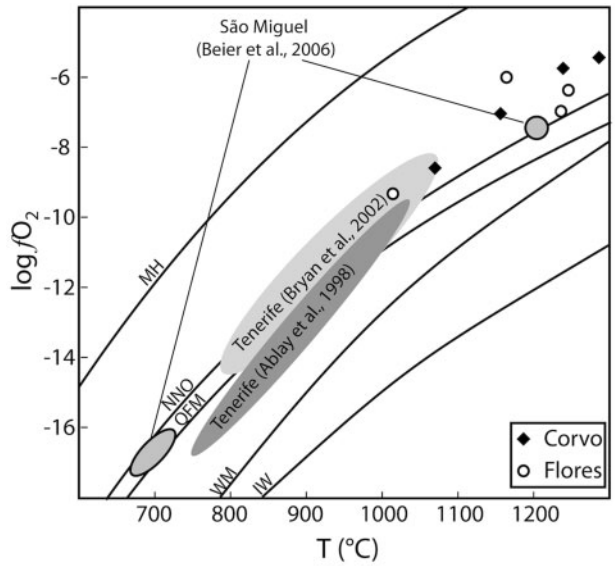

Fig. 17. Log fO_2 vs temperature estimates for lavas from Flores and Corvo. Ulvöspinel–magnetite solid solution experiments from Buddington & Lindsley (1964) were graphically applied to Ti-magnetites for the oxygen fugacity estimates for different lavas. The data are compared with the evolution of pre-caldera lavas from Sete Cidades from São Miguel (Beier *et al.*, 2006), and with lavas from Tenerife (Ablay *et al.*, 1998; Bryan *et al.*, 2002). The Ti-magnetites appear to plot consistently above the NNO buffer, which reflects similar oxidation states for all magmas. MH, magnetite–hematite; NNO, nickel–nickel oxide; QFM, quartz–fayalite–magnetite; WM, wüstite–magnetite; IW, iron–wüstite.

cooling with decreasing pressure, and hence continuous fractionation, becomes apparent in both projections because both island suites cross multiple isotherms with evolving composition (900–700°C). The intersection of the observed lava trend with the temperature contours of Benisek *et al.* (2010) is generally consistent with the cooling of the magmas during ascent, although the anorthoclase temperatures of ~700°C are substantially lower than those inferred from the approach of Fuhrman & Lindsley (1988). It almost appears as if the observed trend of the plagioclases follows an inverse temperature path (i.e. 650–750°C) when applying the models of Fuhrman & Lindsley (1988). Therefore, we also attempted to use the equations described by Putirka (2005) to obtain additional feldspar temperature estimates (Table 4). These estimates result in a good fit to the projected P–T gradient from the clinopyroxene calculations, potentially placing the alkali feldspar crystallization near the surface at Flores (Fig. 16a).

In summary, estimates of the pressure and temperature conditions of crystallization of the lavas from Flores and Corvo have been made using a number of independent methods; the resulting P–T paths, based on the three major phenocryst phases, are internally consistent. A polybaric evolution model is suggested and we infer that fractional crystallization took place during magma ascent in volcanic conduits rather than in a single magma chamber at any specific depth. This conclusion, however, does not negate the existence of magma chambers per se, as the more evolved samples show petrographic (e.g. kaersutite, K-feldspar, large apatite) and morphological (e.g. large caldera on Corvo) features that are readily explained by the existence of a shallow (crustal) magma chamber.

Oxygen fugacity

Lavas containing abundant iron–titanium oxides were used to estimate the oxygen fugacity at the different differentiation stages, and hence at different inferred depths and temperatures. The titanomagnetite mineral chemistry (Table 3) was stoichiometrically evaluated for the various ulvöspinel proportions for comparison with the solid-solution experiments of Buddington & Lindsley (1964). The data are illustrated in Fig. 17 in comparison with studies from Tenerife (Ablay *et al.*, 1998; Bryan *et al.*, 2002) and São Miguel (Beier *et al.*, 2006), which highlight the similarity between these OIB systems. The lavas from Corvo and Flores appear to lie somewhat above the nickel–nickel oxide buffer (NNO). The lavas from Flores may indicate open-system behaviour, as they do not define a buffer-parallel trend. However, the clearer trend of the Corvo samples is consistent with a closed-system fractional crystallization process.

LIQUID LINE OF DESCENT

Primary magma compositions of Flores and Corvo

The major-element trends from Flores and Corvo suggest a similar liquid line of descent for each island coupled with crystallization over a comparable range of depths (Figs 9, 16 and 18). The most primitive samples from each island have MgO contents >11 wt %. However, especially in the case of Corvo, the most MgO-rich lavas show clear petrographic evidence for olivine and clinopyroxene accumulation (refer to Figs 4 and 5, respectively). Mineral analyses from these samples (C-09-10 and C-09-13) reveal that olivine and clinopyroxene are not in equilibrium with the host magma (Table 3). These minerals are most probably accumulated crystals derived from gravitational settling during fractional crystallization. Therefore, these rocks must be ruled out as potential parental or primary magmas.

The most primitive lavas (e.g. whole-rock Mg# = 71, Fig. 5) containing olivine ($Fo_{\sim 88}$, Ni ~ 1750 ppm) and clinopyroxene in equilibrium with their whole-rock compositions are characterized by 10–11 wt % MgO and Ni contents of 200–300 ppm (Tables 1 and 3). Hence, samples C-09-20 and FL-09-41 are considered to resemble near-primary magma compositions for Corvo and Flores, respectively. Although their nickel content may be slightly too low for these to be true primary magmas according to the

criteria of Hess (1992), the model of Hart & Davis (1978) suggests that these samples could reflect near primary magmas formed by ~3% melting of peridotite. The relatively low nickel contents of the olivines and the primitive lavas, however, are consistent with eruption on young and thin lithosphere, as has been described in detail by Niu *et al.* (2011). In the following discussion, these two samples will be used for further investigation of melting and crystallization processes beneath both islands.

Table 5: Primary magma compositions and their P–T *conditions of the Flores and Corvo suites using different model calculations*

	Herzberg & Asimow (2008)		Lee *et al.* (2009)		Putirka (2005)	
	FL-09-41	C-09-20	FL-09-41	C-09-20	FL-09-41	C-09-20
SiO_2	46·3	45·5	46·3	45·4		
TiO_2	1·7	2·0	1·6	2·0		
Al_2O_3	12·4	11·3	12·3	11·2		
Cr_2O_3	0·1	0·1	0·0	0·0		
Fe_2O_3	1·0	1·0	1·0	1·0		
FeO	9·0	9·4	9·0	9·5		
MnO	0·2	0·2	0·2	0·2		
MgO	14·2	15·0	14·8	15·7		
CaO	10·7	11·8	10·5	11·7		
Na_2O	2·9	2·1	2·9	2·0		
K_2O	1·0	0·8	1·0	0·8		
NiO	0·0	0·1				
P_2O_5	0·0	0·3				
H_2O	0·5	0·4	0·5	0·4		
Fo	0·90	0·90	0·90	0·90		
T (°C)	1439	1458	1432	1468	1438	1467
P (GPa)			2·5	2·7		

Primary magma compositions for the parental magma samples C-09-20 and FL-09-41 were calculated following the approach of Lee *et al.* (2009). The corresponding estimated temperature and pressure conditions for basaltic magma generation in the mantle beneath Flores and Corvo are summarized in Fig. 19b and Table 5. The Lee *et al.* (2009) method places constraints for the calculations of MgO > 9 wt %, $Fe^{3+}/Fe^{T} = 0{\cdot}1$ in the basalts and Fo_{90} in the mantle source; hence P–T conditions of equilibration for the parental magmas of five lavas are plotted in Fig. 19a, including the ankaramitic cumulates. A consequence of this analysis is an independent estimate of the amount of H_2O present in the source. The two primary, non-ankaramitic lavas (Fig. 19b) suggest between 0·5 and 1·0% H_2O. Accordingly, our best estimates for the conditions of primary magma generation are just above the spinel–garnet transition of Robinson & Wood (1998) at depths of ~84 km and at a maximum temperature of ~1450°C.

Fractional crystallization

The mineralogy, textures and bulk-rock compositions of the lavas are consistent with fractional crystallization being the dominant differentiation process for both the Corvo and Flores magmatic systems. The decrease in size of the olivine and clinopyroxene phenocrysts (from 20 to 0·5 mm) and the accompanying increase in the size of plagioclase phenocrysts (from 0·5 to 10 mm) with decreasing inferred pressure supports this notion. Moreover, the major-element trends show clear evidence of clinopyroxene-dominated fractionation towards more evolved magma compositions. The first minerals to crystallize from the melt were forsteritic olivine (decrease of MgO accompanied by subtle increase of iron) in minor modal abundance followed by clinopyroxene, which is inferred from the decrease of CaO with decreasing MgO. The latter relationship, together with the flattening trend of

Table 6: Mineral modes extracted from the MELTS models

P (GPa)	T (°C)	1 – F (%)	cpx	ol	plag	spin + mag	apt	Total
12–5·6	1370–1040	70·0	39·4	2·9	3·7	2·6	0·3	49·0
0·1	1210–1010	72·8	29·4	9·3	11·8	2·2	0·2	52·9
0·5	1270–1040	72·6	36·6	6·6	7·0	2·2	0·3	52·7
1·0	1340–1090	69·1	44·8	0·0	0·0	2·7	0·4	47·8
1·5	1410–1150	69·6	46·0	0·0	0·0	1·9	0·4	48·3

The MgO range of the liquid evolution is ~9 wt % in all models. Sample C-09-20 is the starting composition used for all calculations.

Table 7: Partition coefficients used during the Rayleigh-fractionation calculations

	ol	cpx	plag	mag
Cr	0·64	8·49	0·04	150
Ni	32	8·5		29
P	0·038	0·02		
Ti	0·011	0·49	0·1	8
Rb	0·0004	0·00008	0·1	
Sr	0·001	0·113	2·1*	
Y	0	0·34	0·009	
Zr	0·001	0·06	0·003	
Nb	0·00007	0·0012	0·01	
Ba	0·0001	0·0003	0·15*	
La	0·0001	0·03	0·07	
Ce	0·0001	0·057	0·05	
Pr			0·13	
Nd	0·0005	0·14	0·1	
Sm	0·001	0·22	0·06	
Eu			0·73	
Gd		0·3	0·07	
Tb	0·001	0·33	0·06	
Dy	0·0017	0·33	0·06	
Ho	0·0031	0·35	0·05	
Er		0·3	0·05	
Yb	0·05	0·25	0·04	
Lu	0·024	0·31	0·03	
Hf	0·0008	0·12	0·03	
Ta	0·0002	0·0022	0·04	
Pb	0·001	0·008	0·6*	
Th	0·0002	0·007	0·17	
U	0·0003	0·006	0·11	

Olivine (ol) and clinopyroxene (cpx) data from Adam & Green (2006). Plagioclase (plag) data from Aigner-Torres *et al.* (2007). Magnetite (mag) values are estimates based on Esperana *et al.* (1997).
*Data calculated based on Blundy & Wood (1991, 2003).

increase of aluminium with differentiation (Fig. 9d), also suggests that the amount of plagioclase fractionation increases as the liquid evolves. The most evolved lava compositions ($MgO < 3{\cdot}5$ wt %) show petrographic evidence for crystallization of Fe–Ti oxides and apatite and fractionation of these phases as evidenced by decreasing titanium, iron and phosphorus contents (Fig. 9a and f).

The major-element compositions of the lavas from Corvo indicate that the samples lie on a single liquid line of descent. This is not the case for the lavas from Flores. The two sub-parallel trends seen in the Flores major-element data, especially TiO_2 and P_2O_5 versus MgO, suggest similar fractional crystallization histories to the Corvo suite, but different liquid lines of descent. This suggests that not all the samples are of cogenetic origin and that other processes, such as source mixing or (deep) combined fractional crystallization–assimilation (AFC), may be needed to explain the different lava groups on Flores. The occasional appearance of reversely zoned clinopyroxene in some of these lavas may be attributed to such processes.

The major-element data trends do not require that plagioclase is a dominant fractionating phase in the most mafic magmas (Fig. 9); however, it appears to have been crystallizing throughout the range of compositions and apparently accumulated in some magmas from the Flores suite. In the first instance we model the Flores and Corvo suites with a single fractional crystallization model using the MELTS algorithm (Ghiorso & Sack, 1995; Asimow & Ghiorso, 1998).

MELTS modelling

MELTS modelling used 10°C steps and assumed the major-element composition of the inferred parental lava from Corvo (C-09-20) as the starting composition. Intensive parameter inputs of 1375°C at 1·2 GPa were chosen on the basis of the thermobarometric estimates described above. Isobaric models were then calculated at 0·1, 0·5, 1·0 and 1·5 GPa with corresponding liquidus temperatures and compared with a polybaric model constrained by the dP/dT gradient suggested by the Fe–Mg silicates (e.g. Fig. 16). The polybaric model uses the same starting composition as the isobaric models, but starts at an equilibrium pressure of 1·2 GPa and evolves down to 0·56 GPa, along a dP/dT gradient based on the estimates obtained from the geothermobarometric models. The fractionating solids in all models were based on petrographic observations. From the geochemical data and the observed petrology, the following phases are inferred to have crystallized from both the Flores and Corvo magmatic systems: clinopyroxene, olivine, magnetite, ilmenite, plagioclase, apatite (± alkali feldspar, ± amphibole). This is broadly consistent with the fractionating phases determined by MELTS (Table 6).

As illustrated in Fig. 9, the polybaric MELTS model seems to provide the best fit to the observed whole-rock major-element data. This is particularly apparent for the Corvo lavas in Fig. 9a–d. The closest isobaric model for these lavas occurs at 1·0 GPa, which roughly coincides with the depth of the lithosphere–asthenosphere boundary (LAB) beneath the islands (Fig. 18). Nevertheless, this cannot reproduce the low-MgO, low-TiO_2 end of the arrays in Fig. 9a, and storing and fractionating all of the magmas at or near the LAB is unlikely to produce the chemical evolution of the olivine, clinopyroxene and plagioclase phenocrysts observed in the lavas. Conversely, the existence of transitory shallow magma chambers (<0·1 GPa) is indicated by the presence of calderas on

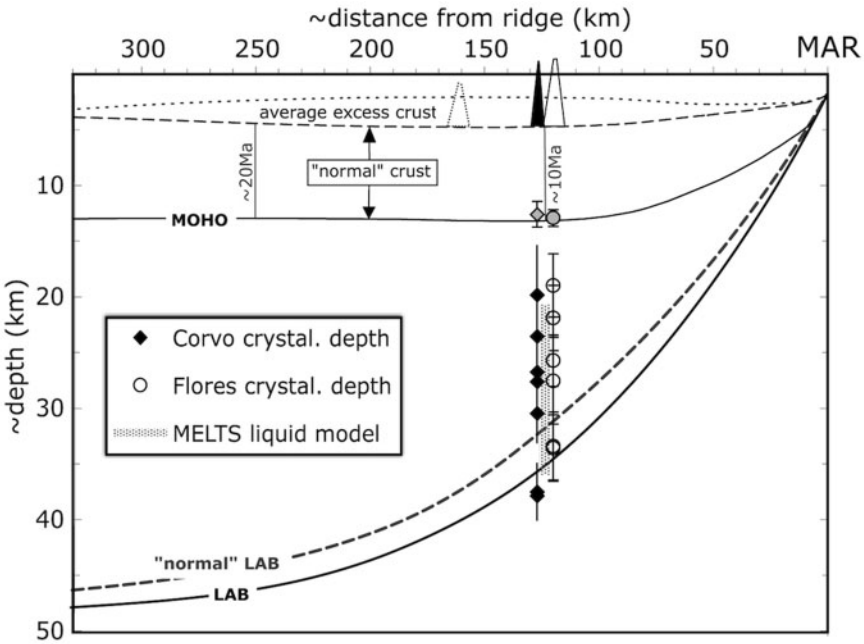

Fig. 18. Schematic cross-section beneath the western Azores plateau (excess crust) indicating the ascent of the crystallizing magmas beneath Flores and Corvo. *P–T* estimates as well as the MELTS liquid model coincide and both imply the onset of crystallization near the lithosphere–asthenosphere boundary (LAB). Stalling of the magmas at the mantle–crust boundary (MOHO) may be inferred from amphibole pressure estimates; however, clinopyroxene-dominated fractionation occurred at greater depths (>0·5 GPa). The volcanic edifices of Flores and Corvo, as well as the submarine seamount ~50 km to the west, are shown at their present-day distance from the MAR.

both islands and is consistent with the presence of low-temperature K-feldspars in the most evolved rocks (<0·8 MgO wt %) on Flores. In summary, we prefer the polybaric differentiation model for Corvo. We note that the Flores data are significantly more scattered. However, there is no reason from the point of view of the mineralogical and major-element data that this model does not equally apply to this island as well.

Trace-element behaviour

The fractional crystallization model calculated using MELTS, and supported by the geothermobarometric estimates, was then further appraised using the trace-element data. Because the observed mineralogy of the basalts is fairly simple in terms of crystallization order, a Rayleigh-fractionation model was used (Fig. 12). Mineral modes for the fractionating assemblage were extracted from the MELTS outputs and cross-checked with the petrography and mineral chemistry. Because the evolution of the magmas is dominated by clinopyroxene fractionation (see caption of Fig. 12), it is not expected that the Rayleigh-fractionation models will discriminate between isobaric and polybaric processes. Clinopyroxene and olivine distribution coefficients were taken from Adam & Green (2006) to best match the highest *P–T* conditions inferred here for the near-primary magmas. However, these have only limited applicability for shallower and cooler conditions and must be treated with caution when calculating the trace-element evolution during fractional crystallization. Appropriate K_D values for Sr, Ba and Pb for plagioclase were calculated following the model of Blundy & Wood (1991) to best represent the anorthite contents of the plagioclase in the more evolved compositions. The work of Aigner-Torres *et al.* (2007) was used for partition coefficients for the remaining trace elements in plagioclase. Magnetite K_D values were estimated based on data provided by Esperança *et al.* (1997). Clinopyroxene and olivine fractionation, however, dominates most strongly at the highest pressures, whereas plagioclase and Fe–Ti oxides are increasingly fractionated towards shallower depths (≪0·5 GPa).

Unfortunately, because the trace-element trends exhibit significant scatter in the Flores lava suite, this exercise does not provide an especially robust test of the MELTS models. Nevertheless, the Rayleigh fractional crystallization model satisfactorily reproduces the trace-element trends with reasonable adherence to the better-defined Corvo data. Because this single-step model (i.e. fixed mineral assemblage) predicts the behaviour of the trace elements over a large range of MgO ($\Delta \sim 9$ wt %), it may be argued that some of the discrepancies between the calculated and observed trend (Fig. 12) are mainly due

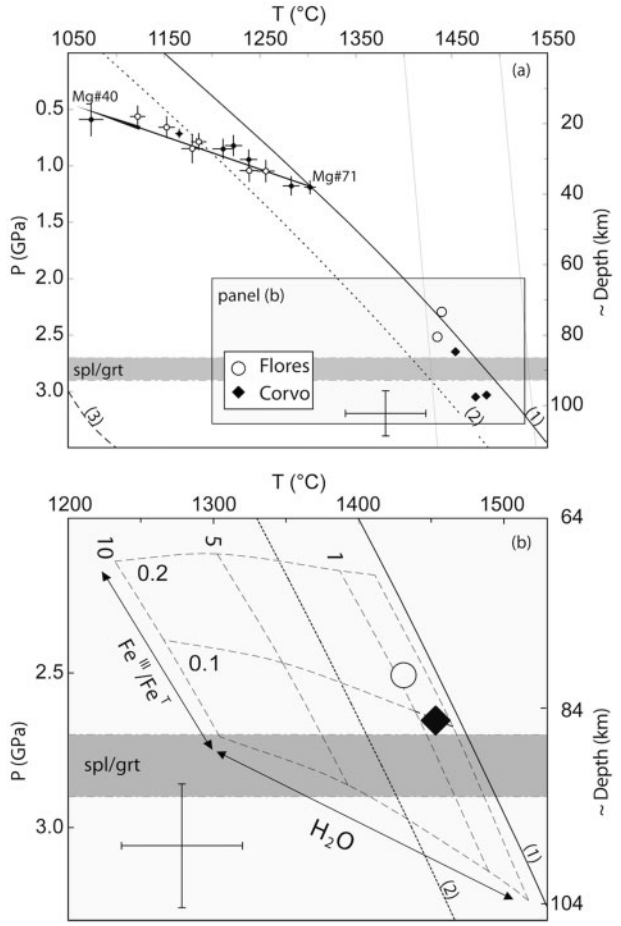

Fig. 19. Temperature and pressure estimates for the generation of the primary melts using the model from Lee *et al.* (2009). The *P–T* path of clinopyroxene crystallization in the lavas is taken from Fig. 16a. The spinel–garnet (Spl/Grt) transition is from Robinson & Wood (1998). Only near-primary magmas (Mg# ~ 70) were used for *P–T* estimates of the primary melts (a). (b) The effect of changing input parameters (e.g. water content and oxidation state) on the estimated *P–T* conditions. The preferred conditions are shown for representative primary magmas from Flores (Fl-09-42) and Corvo (C-09-07). Solidus lines are referenced from (1) Green & Falloon (1998), (2) Katz *et al.* (2003) and (3) Green *et al.* (2010).

to continuous modal changes during the ascent of the crystallizing magma. Alternatively, the discrepancies between the modelled trends and the observed concentrations may be due to the K_D values used and mineral-mode dependence of the crystallization pressures. In the case of Sr, which is compatible in plagioclase and apatite, we observed a linear negative correlation with the pressures extracted from the MELTS model (not shown), and also with the pressures obtained from the clinopyroxene barometry. This relationship may reflect two processes. First, the plagioclase component in the residual liquid gradually increases with decreasing pressure and, second, strontium partitions more strongly into more albite-rich plagioclase as demonstrated by Blundy & Wood (1991). This latter relationship could not be tested sufficiently, as plagioclase becomes efficiently fractionated from the magmas only at shallower levels (≪0·5 GPa), and even then only in minor amounts (~5%).

Figure 12 shows the predicted fractional crystallization trends based on a starting composition assumed to be that of sample C-09-20. The trends of the compatible elements (Ni, Cr) against Nb clearly support clinopyroxene-dominated fractional crystallization as the major process controlling the evolution of both basaltic suites. Again, the scatter in the Flores lavas is probably indicative of other ascent-related processes, such as assimilation. This is even more prominent in the variation of Sr, Y and Zr versus Nb. The low-Nb samples are ankaramitic cumulates. The Corvo sample C-09-17.2 with the lowest Nb concentration indicates clinopyroxene crystallization at depths close to the lithosphere–asthenosphere boundary (Table 4).

In Fig. 14 we compare the MELTS model-based Rayleigh-fractionation model with the variation of Nd/Sr vs Nd and Dy/Yb vs Dy in the lavas. These element pairs were chosen to investigate the relative roles of garnet and plagioclase in the system. The samples with Nd concentrations <20 ppm and Dy <3 ppm are petrologically classified as ankaramitic cumulate rocks. The crystallization model confirms this interpretation because these samples lie on the Corvo fractionation trend at 15·5 and 18·2 wt % MgO. The parental starting composition has a Sr content of ~500 ppm and a Nd content of ~30 ppm (Table 1). As the magmas fractionate to shallower levels the Nd concentration increases as well as the Nd/Sr ratio. Furthermore, two sub-parallel trends for Flores are apparent when compared with Corvo, reflected in variable Nd/Sr at a given Nd concentration (Fig. 14b).

The trends of Dy/Yb versus Dy in Fig. 14a are different between the two islands, but the Dy and Yb concentrations of the most primitive magmas are comparable. The Dy/Yb ratio remains relatively consistent for Corvo, but appears to define two distinct groups for Flores. This may reflect subtle differences in the mantle source beneath Flores and/or some deep fractional crystallization–assimilation process. The differences in the behaviour of these trace elements during magmatic differentiation between the two islands may be explained by temporal variations (e.g. different ascent rates and thus different amounts of assimilated material in some magmas), but also by a difference in the source composition between the two islands.

The polybaric, fractional crystallization model from MELTS is broadly consistent with Rayleigh-fractionation of the trace elements. A total fraction of ~70% of the parental magma is crystallized in the preferred model to explain the most evolved compositions (Table 6). Arguably, crystallization commenced close to the

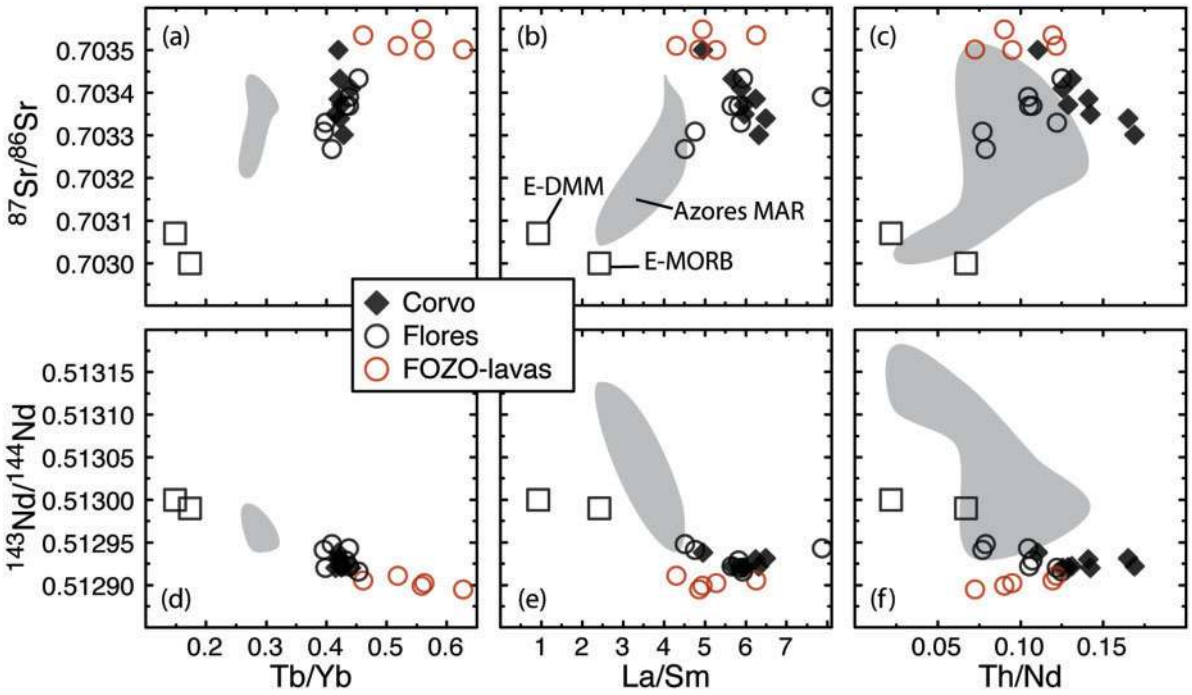

Fig. 20. Strontium and neodymium isotopic compositions for lavas from Flores and Corvo. Panels (a)–(c) highlight the Sr isotopic composition and (d)–(f) the Nd isotopic composition versus garnet signature (Tb/Yb), degree of melting (La/Sm) and source composition (Th/Nd). The field of the Azores MAR is based on data from Bourdon *et al.* (1996) and Dosso *et al.* (1999), and references therein. The red circled Flores samples may represent a common mantle end-member similar to the FOZO mantle reservoir (e.g. Stracke *et al.*, 2005).

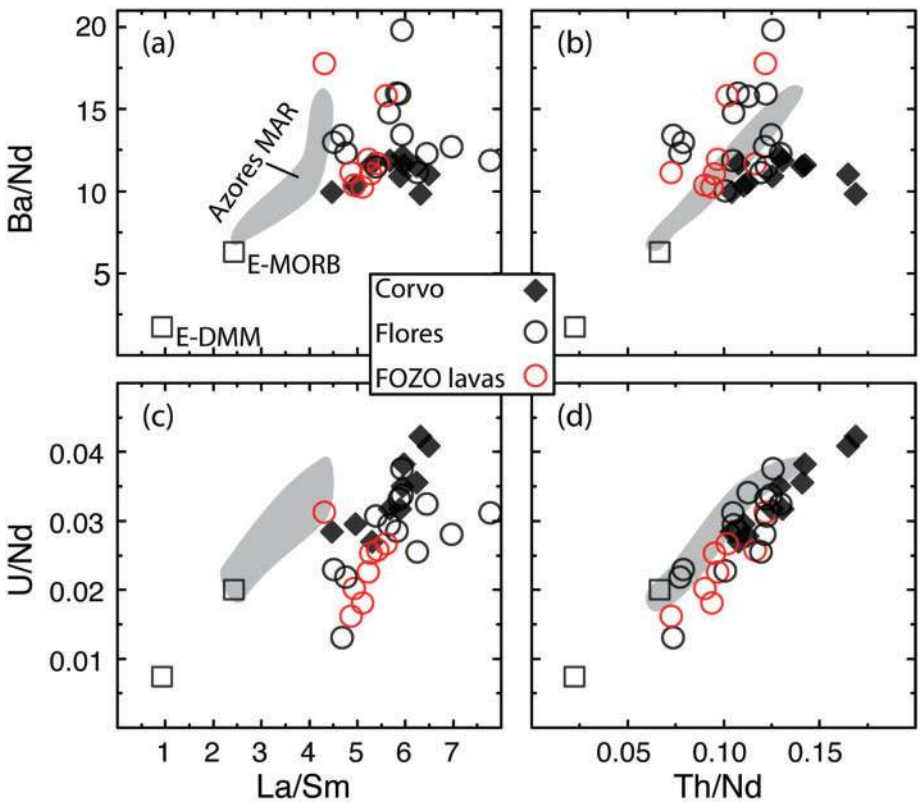

Fig. 21. Variation of Ba/Nd (a, b) and U/Nd (c, d) versus La/Sm and Th/Nd. Red Flores data points reflect the same enriched source as highlighted in Figs 15 and 20. Mantle sources are as follows: E-DMM from Workman & Hart (2005), E-MORB from Sun & McDonough (1989). Panels (a) and (b) illustrate the differences between the Flores and Corvo lava suites. U/Nd (c and d) variations, in contrast, appear to confirm a general mixing trend towards a common enriched mantle source for the two islands.

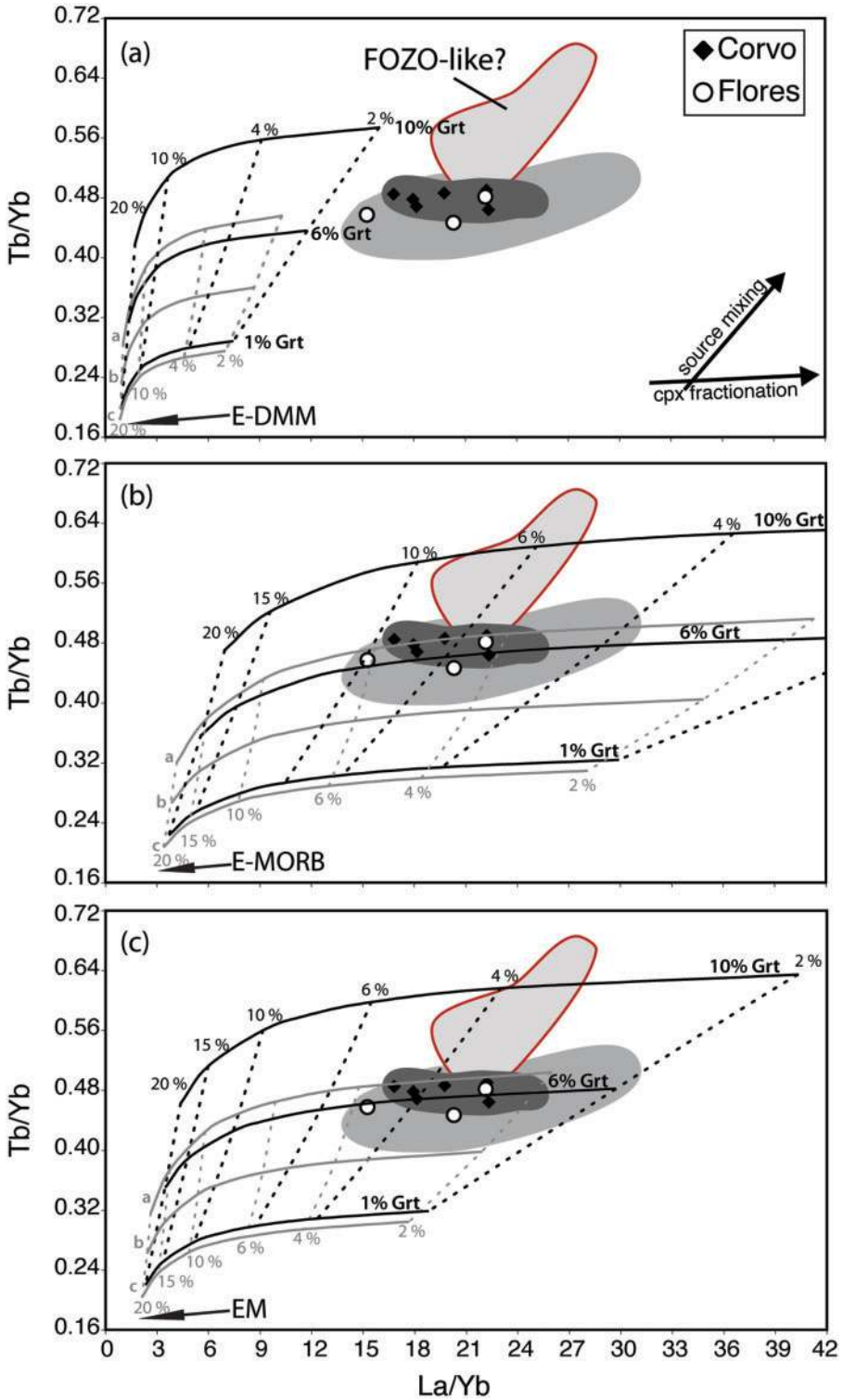

Fig. 22. Tb/Yb versus La/Yb diagrams after Pearce & Parkinson (1993) highlighting the role of garnet and spinel in the melting region. Only primitive samples (Mg# > 65) are plotted for sensitivity purposes; however, the grey fields reflect the general fractionation trends of both islands (dark grey, Corvo; medium and light grey, Flores). Both islands require 3–5% melting of a peridotitic enriched mantle source to produce the primary magmas. The melting models are based on the following parameters: (a) E-DMM from Workman & Hart (2005), (b) E-MORB from Sun & McDonough (1989), (c) EM source from Donnelly *et al.* (2004); batch melting of a peridotite mantle mineralogy with 55% Ol, 25% Opx, 10–19% Cpx, 10–1% Grt, respectively. Garnet was evenly mixed with spinel to further constrain the depth of melting; that is, curve a represents 5% Grt + 5% Spl, b is 3% Grt + 3% Spl and c is 0·5% Grt + 0·5% Spl. The red highlighted Flores field may indicate mixing towards a FOZO-type reservoir (e.g. Stracke *et al.*, 2005). Alternatively, these samples could reflect deeper storage and fractionation at the LAB with associated assimilation.

lithosphere–asthenosphere boundary, the depth of which was calculated using the equations of Parsons & Sclater (1977) and Stein & Stein (1992), illustrated in a geological cross-section in Fig. 18. The onset of crystallization was slightly deeper beneath Corvo (~38 km), although the range of crystallization pressures beneath both islands is inferred to be similar. The occasional appearance of reversely zoned clinopyroxene in some of the Flores lavas may also suggest mixing of more mafic liquid with the crystallizing ascending magmas (e.g. Neumann *et al.*, 1999). Convection in the magma conduits can readily explain some of the observed disequilibrium features, with small-scale stagnation perhaps occurring in magma pockets in sidewalls. Such a model has been invoked for basaltic magma systems previously, especially where there is clear evidence in the evolution of the fractionated mineral assemblages (e.g. Cox & Jamieson, 1974; Cox, 1980; Fram & Lesher, 1997; Nekvasil *et al.*, 2004).

SOURCE COMPOSITION

The P–T conditions in the source region of the melts were constrained through application of the model of Lee *et al.* (2009) and confirmed by calculations based on the work of Herzberg & Asimow (2008); this indicates temperatures and pressures of ~1470°C, 2·7 GPa for Corvo and ~1430°C, 2·5 GPa for Flores (Table 5). These depths are comparable with those inferred for São Miguel, but considerably greater (~15 km deeper) than those for Graciosa, Terceira and João de Castro [compare fig. 11 of Beier *et al.* (2008)].

The mantle source composition beneath Flores and Corvo was evaluated using the radiogenic isotope systematics in combination with key trace-element ratios. Sr and Nd isotope variations are plotted versus key trace-element ratios in Fig. 20 along with data for the MAR basalts in the vicinity of the Azores plateau (Bourdon *et al.*, 1996; Dosso *et al.*, 1999). Most lavas from the two islands overlap on the various plots, but, as described above, there is a group of lavas from Flores with a consistently different composition. These lavas are characterized by Sr–Nd isotope compositions similar to the so-called 'FOZO' mantle reservoir (e.g. Workman *et al.*, 2004; Stracke *et al.*, 2005) and have elevated Tb/Yb ratios (Fig. 20a and d). When combined with plots of Sr and Nd isotopes versus Th/Nd and $(La/Sm)_N$, respectively, it becomes apparent that the bulk of the lavas from the two islands plot between the MAR basalts and the distinct FOZO-like group from Flores (Fig. 20). We note that it is primarily their elevated Sr isotope ratio that distinguishes these latter rocks. This might be attributed to contamination by earlier basalts that evolved to higher $^{87}Sr/^{86}Sr$ during ageing in the lower crust. However, this is precluded by the low Rb/Sr ratios of all of the lavas, coupled with the likely 10 Ma maximum age of the islands. Therefore we conclude that a distinct radiogenic source component ($^{87}Sr/^{86}Sr \sim 0{\cdot}70355$), only observed locally on Flores, was involved during magma generation. The melts from this reservoir are also characterized by relatively high Tb/Yb (>0·55).

On a plot of U/Nd versus Th/Nd (Fig. 21d) the lavas from Flores and Corvo define a mixing trend, in which the data from Corvo extend the trend towards more enriched compositions. The enriched MORB samples from the adjacent MAR (Bourdon *et al.*, 1996; Dosso *et al.*, 1999) are similar to the majority of the Flores lavas in Th/Nd and U/Nd. In contrast, divergent trace-element trends for the two islands are evident on a plot of Ba/Nd versus Th/Nd (Fig. 21b), with the MAR basalts plotting somewhat between the two islands. The relationships in Fig. 21 in general suggest that the MORB-source mantle beneath the MAR (also shown in Fig. 20) is a common end-member from which the lavas from Flores and Corvo extend towards distinct compositions. Thus, three mantle source components, two of which are enriched and one is MORB-source like, appear to be required to explain the compositions of the Flores and Corvo lavas.

Finally, we attempt to constrain the extent of partial melting and the possible role of residual garnet in the source of the Flores and Corvo lavas using a plot of Tb/Yb, largely sensitive to residual garnet, versus La/Yb, which is largely sensitive to the extent of melting (Fig. 22). The three panels in Fig. 22 are contoured for melt fraction using different mantle source compositions from which we infer that around 3–5% melting of an enriched mantle source containing around 5–6% residual garnet (but see below) could explain the primitive lavas from both islands. However, as suggested above, there is a group of Flores lavas that seems to require a different source composition, which is also apparent in the Tb/Yb and La/Yb systematics (see also Figs 20 and 21). These magmas appear to require amounts of garnet that exceed 10% and might be attributed to either deeper melting or mixing with melts from a distinct mantle source.

Despite the above discussion, the implication of Fig. 19 is that melting may not, in fact, reach into the garnet stability zone. To reconcile these apparently conflicting observations, we suggest that the garnet trace-element signature may be inherited. Indeed, because the $^{143}Nd/^{144}Nd$ ratios of all the lavas are consistently higher than CHUR, with epsilon Nd values around +5·5, they must have been derived from mantle source regions that had evolved with time-integrated LREE depletion. However, the degree of LREE enrichment observed in the lavas could not plausibly have been produced by reasonable degrees of melting of a depleted source. Therefore, it seems likely that the LREE enrichment of the lavas reflects recent metasomatism of their source region (e.g. Hawkesworth *et al.*, 1979;

Lustrino *et al.*, 2007). The corollary is that the preceding arguments for the presence and amounts of residual garnet are subject to this caveat and we suggest that melting may not have commenced this deep.

CONCLUSIONS

Lavas from Flores and Corvo provide new constraints on the evolution of the Azores archipelago. New major-element data from these westernmost islands provide evidence for continuous, polybaric, fractional crystallization from the lithosphere–asthenosphere boundary (~38 km depth) to the crust–mantle boundary (~12 km depth). Corvo lavas are, on average, slightly more primitive than those from Flores and constrain initial fractionation assemblages from the presence of ankaramitic cumulate rocks. Corvo lavas require deeper melting conditions at higher temperatures than lavas from Flores. Modelling of the major elements supports the polybaric fractionation model and we propose that no long-lived magma chamber is required to explain the most differentiated lavas, which have ~3 wt % MgO. Only more evolved lavas (<3 wt % MgO) may have formed through stagnation at shallow crustal levels (1–3 km), consistent with the caldera system observed on Corvo.

The Nd–Sr isotope ratios of the Corvo and Flores lavas are similar to those observed amongst the eastern islands of Terceira, Graciosa and western São Miguel, but display a more restricted range. Trace-element ratios (e.g. Nb/Zr, Ta/Hf, La/Sm) suggest the involvement of an enriched source composition that is not observed in the eastern Azores islands or along the Mid-Atlantic Ridge. A discrete mantle component [e.g. high Tb/Yb and lower $(La/Sm)_N$] is seen in a particular lava suite on Flores but is not observed on Corvo, suggesting a limited geographical distribution. We conclude that 3–5% melting of an enriched mantle formed the primary melts underneath Flores and Corvo at depths around 80 km and temperatures around 1450°C. The resultant primary melts commenced to fractionate upon entering the lithosphere, potentially undergoing short-term storage at the lithosphere–asthenosphere boundary. Only small, short-lived magma chambers are interpreted to have existed immediately below the current volcanic edifices.

ACKNOWLEDGEMENTS

V. H. Forjaz and the Observatório Vulcanológico e Geotérmico dos Açores are gratefully acknowledged for their assistance with the sample logistics. B. W. Chappell is thanked for help with the XRF analyses, and P. Wieland for help with the ICP-MS trace-element and TIMS isotope analyses. We thank K. Grant for assisting with the EMP analyses. The paper benefited from constructive reviews by E.-R. Neumann, V. Salters and an anonymous reviewer, which led to great improvement. M. Wilson is thanked for extremely patient editorial handling and helpful comments. This is contribution 169 from the ARC Centre of Excellence for Core to Crust Fluid Systems (http://www.ccfs.mq.edu.au) and 819 in the GEMOC Key Centre (http://www.gemoc.mq.edu.au).

FUNDING

The analytical data were obtained using instrumentation funded by DEST Systemic Infrastructure Grants, ARC LIEF, NCRIS, industry partners and Macquarie University. C. B. was supported by a Feodor-Lynen fellowship from the Alexander von Humboldt-Foundation. S.P.T. was supported by an Australian Research Council Professorial Fellowship (DP0988658).

SUPPLEMENTARY DATA

Supplementary data for this paper are available at *Journal of Petrology* online.

REFERENCES

Abdel-Monem, A. A., Fernandez, L. A. & Boone, G. M. (1975). K–Ar ages from the eastern Azores group (Santa Maria, São Miguel and the Formigas Islands). *Lithos* **8**, 247–254.

Ablay, G. J., Carroll, M. R., Palmer, M. R., Martí, J. & Sparks, R. S. J. (1998). Basanite–phonolite lineages of the Teide–Pico Viejo volcanic complex, Tenerife, Canary Islands. *Journal of Petrology* **39**, 905–936.

Adam, J. & Green, T. (2006). Trace element partitioning between mica- and amphibole-bearing garnet lherzolite and hydrous basanitic melt: 1. Experimental results and the investigation of controls on partitioning behaviour. *Contributions to Mineralogy and Petrology* **152**, 1–17.

Aigner-Torres, M., Blundy, J. D., Ulmer, P. & Pettke, T. (2007). Laser ablation ICPMS study of trace element partitioning between plagioclase and basaltic melts: an experimental approach. *Contributions to Mineralogy and Petrology* **153**, 647–667.

Asimow, P. D. & Ghiorso, M. S. (1998). Algorithmic modifications extending MELTS to calculate subsolidus phase relations. *American Mineralogist* **83**, 1127–1132.

Azevedo, J. M. M. & Ferreira, M. R. P. (1999). Volcanic gaps and subaerial records of palaeo-sea-levels on Flores Island (Azores): tectonic and morphological implications. *Journal of Geodynamics* **28**, 117–129.

Azevedo, J. M. M. & Ferreira, M. R. P. (2006). The volcanotectonic evolution of Flores Island, Azores (Portugal). *Journal of Volcanology and Geothermal Research* **156**, 90–102.

Baptista, P., Osório, J., Bastos, L., Fernandes, R. & Borges, F. S. (1999). Aplicação de técnicas geodésicas ao estudo do comportamento geodinâmico actual da Junção Tripla dos Açores. *GEOlogos* **5**, 1–12.

Beattie, P. (1993). Olivine–melt and orthopyroxene–melt equilibria. *Contributions to Mineralogy and Petrology* **115**, 103–111.

Beier, C., Haase, K. M. & Hansteen, T. H. (2006). Magma evolution of the Sete Cidades volcano, São Miguel, Azores. *Journal of Petrology* **47**, 1375–1411.

Beier, C., Stracke, A. & Haase, K. M. (2007). The peculiar geochemical signatures of São Miguel (Azores) lavas: Metasomatised or recycled mantle sources? *Earth and Planetary Science Letters* **259**, 186–199.

Beier, C., Haase, K. M., Abouchami, W., Krienitz, M.-S. & Hauff, F. (2008). Magma genesis by rifting of oceanic lithosphere above anomalous mantle: Terceira Rift, Azores. *Geochemistry, Geophysics, Geosystems* **9**, Q12013.

Beier, C., Turner, S., Plank, T. & White, W. (2010). A preliminary assessment of the symmetry of source composition and melting dynamics across the Azores plume. *Geochemistry, Geophysics, Geosystems* **11**, Q02004.

Benisek, A., Kroll, H. & Cemic, L. (2004). New developments in two-feldspar thermometry. *American Mineralogist* **89**, 1496–1504.

Benisek, A., Dachs, E. & Kroll, H. (2010). A ternary feldspar-mixing model based on calorimetric data: development and application. *Contributions to Mineralogy and Petrology* **160**, 327–337.

Blundy, J. D. & Wood, B. J. (1991). Crystal-chemical controls on the partitioning of Sr and Ba between plagioclase feldspar, silicate melts, and hydrothermal solutions. *Geochimica et Cosmochimica Acta* **55**, 193–209.

Blundy, J. & Wood, B. (2003). Partitioning of trace elements between crystals and melts. *Earth and Planetary Science Letters* **210**, 383–397.

Bourdon, B., Langmuir, C. H. & Zindler, A. (1996). Ridge–hotspot interaction along the Mid-Atlantic Ridge between 37°30' and 40°30'N: the U–Th disequilibrium evidence. *Earth and Planetary Science Letters* **142**, 175–189.

Bryan, S. E., Martí, J. & Leosson, M. (2002). Petrology and geochemistry of the Bandas del Sur Formation, Las Cañadas edifice, Tenerife (Canary Islands). *Journal of Petrology* **43**, 1815–1856.

Buddington, A. F. & Lindsley, D. H. (1964). Iron–titanium oxide minerals and synthetic equivalents. *Journal of Petrology* **5**, 310–357.

Cannat, M., Briais, A., Deplus, C., Escartín, J., Georgen, J., Lin, J., Mercouriev, S., Meyzen, C., Muller, M., Pouliquen, G., Rabain, A. & da Silva, P. (1999). Mid-Atlantic Ridge–Azores hotspot interactions: along-axis migration of a hotspot-derived event of enhanced magmatism 10 to 4 Ma ago. *Earth and Planetary Science Letters* **173**, 257–269.

Charlou, J. L., Donval, J. P., Douville, E., Jean-Baptiste, P., Radford-Knoery, J., Fouquet, Y., Dapoigny, A. & Stievenard, M. (2000). Compared geochemical signatures and the evolution of Menez Gwen (37°50'N) and Lucky Strike (37°17'N) hydrothermal fluids, south of the Azores Triple Junction on the Mid-Atlantic Ridge. *Chemical Geology* **171**, 49–75.

Chauvel, C. & Blichert-Toft, J. (2001). A hafnium isotope and trace element perspective on melting of the depleted mantle. *Earth and Planetary Science Letters* **190**, 137–151.

Chen, C.-Y. & Frey, F. A. (1983). Origin of Hawaiian tholeiite and alkalic basalt. *Nature* **302**, 785–789.

Clague, D. A. (1987). Hawaiian alkaline volcanism. In: Fitton, J. G. & Upton, B. G. J. (eds) *Alkaline Igneous Rocks. Geological Society, London, Special Publications* **30**, 227–252.

Claude-Ivanaj, C., Joron, J.-L. & Allègre, C. J. (2001). ^{238}U–^{230}Th–^{226}Ra fractionation in historical lavas from the Azores: long-lived source heterogeneity vs. metasomatism fingerprints. *Chemical Geology* **176**, 295–310.

Cox, K. G. (1980). A model for flood basalt vulcanism. *Journal of Petrology* **21**, 629–650.

Cox, K. G. & Jamieson, B. G. (1974). The olivine-rich lavas of Nuanetsi: a study of polybaric magmatic evolution. *Journal of Petrology* **15**, 269–301.

Deer, W. A., Howie, R. A. & Zussman, J. (1992). *An Introduction to the Rock-forming Minerals*. Harlow: Pearson.

Donnelly, K. E., Goldstein, S. L., Langmuir, C. H. & Spiegelman, M. (2004). Origin of enriched ocean ridge basalts and implications for mantle dynamics. *Earth and Planetary Science Letters* **226**, 347–366.

Dosso, L., Bougault, H., Langmuir, C. H., Bollinger, C., Bonnier, O. & Etoubleau, J. (1999). The age and distribution of mantle heterogeneity along the Mid-Atlantic Ridge (31–41°N). *Earth and Planetary Science Letters* **170**, 269–286.

Droop, G. T. R. (1987). A general equation for estimating Fe^{3+} concentrations in ferromagnesian silicates and oxides from microprobe analyses, using stoichiometric criteria. *Mineralogical Magazine* **51**, 431–435.

Dupré, B., Lambret, B. & Allègre, C. J. (1982). Isotopic variations within a single oceanic island: the Terceira case. *Nature* **299**, 620–622.

Eggins, S. M., Woodhead, J. D., Kinsley, L. P. J., Mortimer, G. E., Sylvester, P., McCulloch, M. T., Hergt, J. M. & Handler, M. R. (1997). A simple method for the precise determination of ≥40 trace elements in geological samples by ICPMS using enriched isotope internal standardisation. *Chemical Geology* **134**, 311–326.

Esperança, S., Carlson, R. W., Shirey, S. B. & Smith, D. (1997). Dating crust–mantle separation: Re–Os isotopic study of mafic xenoliths from central Arizona. *Geology* **25**, 651–654.

Fernandes, R. M. S., Bastos, L., Miranda, J. M., Lourenço, N., Ambrosius, B. A. C., Noomen, R. & Simons, W. (2006). Defining the plate boundaries in the Azores region. *Journal of Volcanology and Geothermal Research* **156**, 1–9.

Flower, M. F. J., Schmincke, H. U. & Bowman, H. (1976). Rare earth and other trace elements in historic azorean lavas. *Journal of Volcanology and Geothermal Research* **1**, 127–147.

Fram, M. S. & Lesher, C. E. (1997). Generation and polybaric differentiation of East Greenland Early Tertiary flood basalts. *Journal of Petrology* **38**, 231–275.

França, Z., Lago, M., Nunes, J. C., Gale, C., Forjaz, V. H., Pueyo, O. & Arranz, E. (2006*a*). Geochemistry of alkaline basalts of Corvo Island (Azores, Portugal): preliminary data. *Geogaceta* **40**, 87–90.

França, Z. T. M., Tassinari, C. C. G., Cruz, J. V., Aparicio, A. Y., Araña, V. & Rodrigues, B. N. (2006*b*). Petrology, geochemistry and Sr–Nd–Pb isotopes of the volcanic rocks from Pico Island–Azores (Portugal). *Journal of Volcanology and Geothermal Research* **156**, 71–89.

França, Z., Lago, M., Gale, C., Ubide, T., Widom, E., Arranz, E. & Forjaz, V. H. (2008). Composition of gabbroic xenoliths in Flores Island (Azores, Portugal). *Revista de la Sociedad Española de Mineralogía* **9**, 103–104.

Fuhrman, M. L. & Lindsley, D. H. (1988). Ternary-feldspar modeling and thermometry. *American Mineralogist* **73**, 201–215.

Gente, P., Dyment, J. R. M., Maia, M. & Goslin, J. (2003). Interaction between the Mid-Atlantic Ridge and the Azores hot spot during the last 85 Myr: Emplacement and rifting of the hot spot-derived plateaus. *Geochemistry, Geophysics, Geosystems* **4**, Q8514.

Georgen, J. E. (2008). Mantle flow and melting beneath oceanic ridge–ridge–ridge triple junctions. *Earth and Planetary Science Letters* **270**, 231–240.

Georgen, J. E. & Sankar, R. D. (2010). Effects of ridge geometry on mantle dynamics in an oceanic triple junction region: Implications for the Azores Plateau. *Earth and Planetary Science Letters* **298**, 23–34.

Ghiorso, M. S. & Sack, R. O. (1995). Chemical mass transfer in magmatic processes IV. A revised and internally consistent thermodynamic model for the interpolation and extrapolation of liquid–solid equilibria in magmatic systems at elevated temperatures and pressures. *Contributions to Mineralogy and Petrology* **119**, 197–212.

Green, D. H. & Falloon, T. J. (1998). Pyrolite: A Ringwood concept and its current expression. In: Jackson, I. N. S. (ed.) *The Earth's Mantle; Composition, Structure, and Evolution*. Cambridge: Cambridge University Press, pp. 311–378.

Green, D. H., Hibberson, W. O., Kovacs, I. & Rosenthal, A. (2010). Water and its influence on the lithosphere–asthenosphere boundary. *Nature* **467**, 448–451.

Gudmundsson, A. (2000). Dynamics of volcanic systems in Iceland: example of tectonism and volcanism at juxtaposed hot spot and mid-ocean ridge systems. *Annual Review of Earth and Planetary Sciences* **28**, 107–140.

Haase, K. M. & Beier, C. (2003). Tectonic control of ocean island basalt sources on São Miguel, Azores? *Geophysical Research Letters* **30**, doi:10.1029/2003GL017500.

Hansteen, T. H., Klügel, A. & Schmincke, H.-U. (1998). Multi-stage magma ascent beneath the Canary Islands: evidence from fluid inclusions. *Contributions to Mineralogy and Petrology* **132**, 48–64.

Hart, S. R. & Davis, K. E. (1978). Nickel partitioning between olivine and silicate melt. *Earth and Planetary Science Letters* **40**, 203–219.

Hawkesworth, C. J., Norry, M. J., Roddick, J. C. & Vollmer, R. (1979). $^{143}Nd/^{144}Nd$ and $^{87}Sr/^{86}Sr$ ratios from the Azores and their significance in LIL-element enriched mantle. *Nature* **280**, 28–31.

Herzberg, C. & Asimow, P. D. (2008). Petrology of some oceanic island basalts: PRIMELT2.XLS software for primary magma calculation. *Geochemistry, Geophysics, Geosystems* **9**, Q09001.

Hess, P. (1992). Phase equilibria constraints on the origin of ocean floor basalts. In: Phipps Morgan, J., Blackman, D. K. & Sinton, J. M. (eds) *Mantle Flow and Melt Generation at Mid-Ocean Ridges. Geophysical Monographs, American Geophysical Union* **71**, 67–102.

Jochum, K. P. & Nohl, U. (2008). Reference materials in geochemistry and environmental research and the GeoReM database. *Chemical Geology* **253**, 50–53.

Katz, R. F., Spiegelman, M. & Langmuir, C. H. (2003). A new parameterization of hydrous mantle melting. *Geochemistry, Geophysics, Geosystems* **4**, 1073.

Kingsley, R. H. & Schilling, J.-G. (1995). Carbon in Mid-Atlantic Ridge basalt glasses from 28°N to 63°N: Evidence for a carbon-enriched Azores mantle plume. *Earth and Planetary Science Letters* **129**, 31–53.

Klügel, A., Hoernle, K. A., Schmincke, H.-U. & White, J. D. L. (2000). The chemically zoned 1949 eruption on La Palma (Canary Islands): Petrologic evolution and magma supply dynamics of a rift zone eruption. *Journal of Geophysical Research* **105**, 5997–6016.

Kokfelt, T. F., Hoernle, K., Lundstrom, C., Hauff, F. & van den Bogaard, C. (2009). Time-scales for magmatic differentiation at the Snaefellsjökull central volcano, western Iceland: Constraints from U–Th–Pa–Ra disequilibria in post-glacial lavas. *Geochimica et Cosmochimica Acta* **73**, 1120–1144.

Krause, D. C. & Watkins, N. D. (1970). North Atlantic crustal genesis in the vicinity of the Azores. *Geophysical Journal of the Royal Astronomical Society* **19**, 261–283.

Lee, C.-T. A., Luffi, P., Plank, T., Dalton, H. & Leeman, W. P. (2009). Constraints on the depths and temperatures of basaltic magma generation on Earth and other terrestrial planets using new thermobarometers for mafic magmas. *Earth and Planetary Science Letters* **279**, 20–33.

Le Maitre, R. W., Bateman, P., Dudek, A., Keller, J., LeBas, M. J., Sabine, P. A., Schmid, R., Sorensen, H., Streckeiesn, A., Woolley, A. R. & Zanettin, B. (1989). *A Classification of Igneous Rocks and Glossary of Terms*. Oxford: Blackwell.

Lindsley, D. H. (1983). Pyroxene thermometry. *American Mineralogist* **68**, 477–493.

Luis, J. F., Miranda, J. M., Galdeano, A. & Patriat, P. (1998). Constraints on the structure of the Azores spreading center from gravity data. *Marine Geophysical Researches* **20**, 157–170.

Lustrino, M., Melluso, L. & Morra, V. (2007). The geochemical peculiarity of 'Plio-Quaternary' volcanic rocks of Sardinia in the circum-Mediterranean area. In: Beccaluva, L., Bianchini, G. & Wilson, M. (eds) Cenozoic Volcanism in the Mediterranean Area: *Geological Society of America Special Papers* **418**, 277–301.

Macdonald, G. A. (1968). Composition of Hawaiian lavas. In: Coats, R. R., Hay, R. L. & Anderson, C. A. (eds) *Studies in Volcanology: A Memoir in Honor of Howel Williams*. Boulder, CO: Geological Society of America, pp. 477–522.

Madeira, J. & Ribeiro, A. (1990). Geodynamic models for the Azores triple junction: A contribution from tectonics. *Tectonophysics* **184**, 405–415.

Madureira, P., Moreira, M., Mata, J. & Allègre, C. J. (2005). Primitive neon isotopes in Terceira Island (Azores archipelago). *Earth and Planetary Science Letters* **233**, 429–440.

Millet, M.-A., Doucelance, R., Baker, J. A. & Schiano, P. (2009). Reconsidering the origins of isotopic variations in Ocean Island Basalts: Insights from fine-scale study of São Jorge Island, Azores archipelago. *Chemical Geology* **265**, 289–302.

Montelli, R., Nolet, G., Dahlen, F. A., Masters, G., Engdahl, E. R. & Hung, S.-H. (2004). Finite-frequency tomography reveals a variety of plumes in the mantle. *Science* **303**, 338–343.

Moreira, M., Doucelance, R., Kurz, M. D., Dupré, B. & Allègre, C. J. (1999). Helium and lead isotope geochemistry of the Azores Archipelago. *Earth and Planetary Science Letters* **169**, 189–205.

Nekvasil, H., Dondolini, A., Horn, J., Filiberto, J., Long, H. & Lindsley, D. H. (2004). The origin and evolution of silica-saturated alkalic suites: an experimental study. *Journal of Petrology* **45**, 693–721.

Neumann, E.-R., Wulff-Pedersen, E., Simonsen, S. L., Pearson, N. J., Martí, J. & Mitjavila, J. (1999). Evidence for fractional crystallization of periodically refilled magma chambers in Tenerife, Canary Islands. *Journal of Petrology* **40**, 1089–1123.

Niu, Y., Wilson, M., Humphreys, E. R. & O'Hara, M. J. (2011). The origin of intra-plate ocean island basalts (OIB): the lid effect and its geodynamic implications. *Journal of Petrology* **52**, 1443–1468.

Nunes, J. C., Camacho, A., França, Z., Montesinos, F. G., Alves, M., Vieira, R., Velez, E. & Ortiz, E. (2006). Gravity anomalies and crustal signature of volcano–tectonic structures of Pico Island (Azores). *Journal of Volcanology and Geothermal Research* **156**, 55–70.

Parsons, B. & Sclater, J. G. (1977). An analysis of the variation of ocean floor bathymetry and heat flow with age. *Journal of Geophysical Research* **82**, 803–827.

Pearce, J. A. & Parkinson, I. J. (1993). Trace element models for mantle melting: application to volcanic arc petrogenesis. In: Prichard, H. M., Alabaster, T., Harris, N. B. W. & Neary, C. R. (eds) *Magmatic Processes and Plate Tectonics. Geological Society, London, Special Publications* **76**, 373–403.

Pin, C. & Zalduegui, J. S. (1997). Sequential separation of light rare-earth elements, thorium and uranium by miniaturized extraction chromatography: Application to isotopic analyses of silicate rocks. *Analytica Chimica Acta* **339**, 79–89.

Potts, P. J., Webb, P. C. & Watson, J. S. (1984). Energy-dispersive X-ray fluorescence analysis of silicate rocks for major and trace elements. *X-Ray Spectrometry* **13**, 2–15.

Presnall, D. C., Dixon, S. A., Dixon, J. R., O'Donnell, T. H., Brenner, N. L., Schrock, R. L. & Dycus, D. W. (1978). Liquidus phase relations on the join diopside–forsterite–anorthite from 1 atm to 20 kbar: Their bearing on the generation and crystallisation

of basaltic magma. *Contributions to Mineralogy and Petrology* **66**, 203–220.

Prytulak, J. & Elliott, T. (2009). Determining melt productivity of mantle sources from ^{238}U–^{230}Th and ^{235}U–^{231}Pa disequilibria; an example from Pico Island, Azores. *Geochimica et Cosmochimica Acta* **73**, 2103–2122.

Putirka, K. D. (1999). Clinopyroxene + liquid equilibria to 100 kbar and 2450 K. *Contributions to Mineralogy and Petrology* **135**, 151–163.

Putirka, K. D., Ryerson, F. J. & Mikaelian, H. (2003). New igneous thermobarometers for mafic and evolved lava compositions, based on clinopyroxene + liquid equilibria. *American Mineralogist* **88**, 1542–1554.

Putirka, K. D. (2005). Igneous thermometers and barometers based on plagioclase + liquid equilibria: Tests of some existing models and new calibrations. *American Mineralogist* **90**, 336–346.

Putirka, K. D. (2008). Thermometers and barometers for volcanic systems. In: Putirka, K. D. & Tepley, F. J., III (eds) *Minerals, Inclusions and Volcanic Processes. Mineralogical Society of America and Geochemical Society, Reviews in Mineralogy and Geochemistry* **69**, 61–120.

Rhodes, J. M., Dungan, M. A., Blanchard, D. P. & Long, P. E. (1979). Magma mixing at mid-ocean ridges: Evidence from basalts drilled near 22°N on the Mid-Atlantic Ridge. *Tectonophysics* **55**, 35–61.

Ridolfi, F., Renzulli, A. & Puerini, M. (2010). Stability and chemical equilibrium of amphibole in calc-alkaline magmas: an overview, new thermobarometric formulations and application to subduction-related volcanoes. *Contributions to Mineralogy and Petrology* **160**, 45–66.

Robinson, J. A. C. & Wood, B. J. (1998). The depth of the spinel to garnet transition at the peridotite solidus. *Earth and Planetary Science Letters* **164**, 277–284.

Ryall, P., Blanchard, M. C. & Medioli, F. (1983). A subsided island west of Flores. *Canadian Journal of Earth Sciences* **20**, 764–775.

Schaefer, B. F., Turner, S., Parkinson, I., Rogers, N. & Hawkesworth, C. (2002). Evidence for recycled Archaean oceanic mantle lithosphere in the Azores plume. *Nature* **420**, 304–307.

Schwarz, S., Klügel, A. & Wohlgemuth-Ueberwasser, C. (2004). Melt extraction pathways and stagnation depths beneath the Madeira and Desertas rift zones (NE Atlantic) inferred from barometric studies. *Contributions to Mineralogy and Petrology* **147**, 228–240.

Searle, R. (1980). Tectonic pattern of the Azores spreading centre and triple junction. *Earth and Planetary Science Letters* **51**, 415–434.

Shorttle, O., Maclennan, J. & Jones, S. M. (2010). Control of the symmetry of plume–ridge interaction by spreading ridge geometry. *Geochemistry, Geophysics, Geosystems* **11**, Q0AC05.

Skovgaard, A. C., Storey, M., Baker, J., Blusztajn, J. & Hart, S. R. (2001). Osmium–oxygen isotopic evidence for a recycled and strongly depleted component in the Iceland mantle plume. *Earth and Planetary Science Letters* **194**, 259–275.

Sleep, N. H. (1990). Hotspots and mantle plumes: some phenomenology. *Journal of Geophysical Research* **95**, 6715–6736.

Sleep, N. H. (2006). Mantle plumes from top to bottom. *Earth-Science Reviews* **77**, 231–271.

Sobolev, A. V., Hofmann, A. W., Sobolev, S. V. & Nikogosian, I. K. (2005). An olivine-free mantle source of Hawaiian shield basalts. *Nature* **434**, 590–597.

Stein, C. A. & Stein, S. (1992). A model for the global variation in oceanic depth and heat flow with lithospheric age. *Nature* **359**, 123–129.

Stolper, E. (1980). A phase diagram for mid-ocean ridge basalts: Preliminary results and implications for petrogenesis. *Contributions to Mineralogy and Petrology* **74**, 13–27.

Stracke, A., Hofmann, A. W. & Hart, S. R. (2005). FOZO, HIMU, and the rest of the mantle zoo. *Geochemistry, Geophysics, Geosystems* **6**, Q05007.

Sun, S. s. & McDonough, W. F. (1989). Chemical and isotopic systematics of oceanic basalts: implications for mantle composition and processes. In: Saunders, A. D. & Norry, M. J. (eds) *Magmatism in the Ocean Basins. Geological Society, London, Special Publications* **42**, 313–345.

Turner, S., Hawkesworth, C., Rogers, N. & King, P. (1997). U–Th isotope disequilibria and ocean island basalt generation in the Azores. *Chemical Geology* **139**, 145–164.

Turner, S., Tonarini, S., Bindeman, I., Leeman, W. P. & Schaefer, B. F. (2007). Boron and oxygen isotope evidence for recycling of subducted components over the past 2·5 Gyr. *Nature* **447**, 702–705.

Vernon, R. H. (2004). *A Practical Guide to Rock Microstructure*. Cambridge: Cambridge University Press.

Vogt, P. R. & Jung, W. Y. (2004). The Terceira Rift as hyper-slow, hotspot-dominated oblique spreading axis: A comparison with other slow-spreading plate boundaries. *Earth and Planetary Science Letters* **218**, 77–90.

Watson, S. & McKenzie, D. (1991). Melt generation by plumes: a study of Hawaiian volcanism. *Journal of Petrology* **32**, 501–537.

Wessel, P. & Smith, W. H. F. (1991). Free software helps map and display data. *EOS Transactions, American Geophysical Union* **72**, 441.

Wessel, P. & Smith, W. H. F. (1995). New version of the Generic Mapping Tools released. *EOS Transactions, American Geophysical Union***79**, 579.

Whipkey, C. E., Capo, R. C., Chadwick, O. A. & Stewart, B. W. (2000). The importance of sea spray to the cation budget of a coastal Hawaiian soil: a strontium isotope approach. *Chemical Geology* **168**, 37–48.

White, W. M., Tapia, M. D. M. & Schilling, J. G. (1979). The petrology and geochemistry of the Azores Islands. *Contributions to Mineralogy and Petrology* **69**, 201–213.

Widom, E., Schmincke, H. U. & Gill, J. B. (1992). Processes and timescales in the evolution of a chemically zoned trachyte: Fogo A, São Miguel, Azores. *Contributions to Mineralogy and Petrology* **111**, 311–328.

Woodhead, J. D. (1992). Temporal geochemical evolution in oceanic intra-plate volcanics: a case study from the Marquesas (French Polynesia) and comparison with other hotspots. *Contributions to Mineralogy and Petrology* **111**, 458–467.

Workman, R. K. & Hart, S. R. (2005). Major and trace element composition of the depleted MORB mantle (DMM). *Earth and Planetary Science Letters* **231**, 53–72.

Workman, R. K., Hart, S. R., Jackson, M., Regelous, M., Farley, K. A., Blusztajn, J., Kurz, M. & Staudigel, H. (2004). Recycled metasomatized lithosphere as the origin of the Enriched Mantle II (EM2) end-member: Evidence from the Samoan Volcanic Chain. *Geochemistry, Geophysics, Geosystems* **5**, Q04008.

Yu, D., Fontignie, D. & Schilling, J.-G. (1997). Mantle plume–ridge interactions in the Central North Atlantic: A Nd isotope study of Mid-Atlantic Ridge basalts from 30°N to 50°N. *Earth and Planetary Science Letters* **146**, 259–272.

Zhao, D. (2007). Seismic images under 60 hotspots: Search for mantle plumes. *Gondwana Research* **12**, 335–355.